



# 1 **Catchment power and the joint distribution of elevation** 2 **and travel distance to the outlet.**

3 Leonard S. Sklar<sup>1</sup>, Clifford S. Riebe<sup>2</sup>, Claire E. Lukens<sup>2</sup>, Dino Bellugi<sup>3</sup>

4 <sup>1</sup>Department of Earth & Climate Sciences, San Francisco State University, San Francisco, CA 94132 USA

5 <sup>2</sup>Department of Geology and Geophysics, University of Wyoming, Laramie, WY 82071 USA

6 <sup>3</sup>Department of Earth, Atmospheric and Planetary Sciences, MIT, Cambridge, MA 02139 USA

7 Correspondence to L.S. Sklar (leonard@sfsu.edu)

8 **Abstract** The delivery of water, sediment and solutes by catchments is influenced by the distribution of  
9 source elevations and their travel distances to the outlet. For example, elevation affects the magnitude and  
10 phase of precipitation, as well as the climatic factors that govern rock weathering, which influence the  
11 production rate and initial particle size of sediments. Travel distance, in turn, affects the timing of flood  
12 peaks at the outlet and the degree of sediment size reduction by wear, which affect particle size  
13 distributions at the outlet. The distributions of elevation and travel distance have been studied extensively  
14 but separately, as the hypsometric curve and width function. Yet a catchment can be considered as a  
15 collection of points, each with paired values of elevation and travel distance. For every point, the ratio of  
16 elevation to travel distance defines the mean slope for transport of mass to the outlet. Recognizing that  
17 mean slope is proportional to the average rate of loss of potential energy by water and sediment during  
18 transport to the outlet, we use the joint distribution of elevation and travel distance to define two new  
19 metrics for catchment geometry: “source-area power,” and the corresponding catchment-wide integral  
20 “catchment power.” We explore patterns in source-area and catchment power across three study catchments  
21 spanning a range of relief and drainage area. We then develop an empirical algorithm for generating  
22 synthetic source-area power distributions, which can be parameterized with data from natural catchments,  
23 and used to explore the effects of topography on the distribution on fluxes of water, sediment, isotopes and  
24 other landscape products passing through catchment outlets. This new way of quantifying the three-  
25 dimensional geometry of catchments may provide a fresh perspective on problems of both practical and  
26 theoretical interest.

## 27 **1. Introduction**

28 The physical and ecological dynamics of rivers are influenced by upstream sources of water,  
29 solutes, and sediment. These materials are produced at rates that vary from source to source depending on  
30 factors such as precipitation, weathering, erosion, and ecosystem productivity. Spatial variations in these  
31 factors commonly correspond to differences in elevation. For example, elevation influences both the  
32 magnitude and phase of precipitation (Roe, 2005; Minder et al., 2011), the climatic factors that govern rock  
33 weathering (White and Blum, 1995; Riebe et al., 2004), the particle size and production rate of sediment  
34 from slopes (Marshall and Sklar, 2012; Riebe et al., 2015), and both the distribution of biomes (Lomolino,



35 2001) and their net primary productivity (Raich et al., 1997). Thus elevation is a fundamental characteristic  
36 of the source areas that supply water, solutes, and sediment to catchment outlets.

37 Along the journey from source to outlet, material is mixed together with products of other sources  
38 and altered by chemical, physical, and biological processes. The mixing and alteration of materials depends  
39 in part on the travel distance between the source and outlet. For example, travel distance influences the  
40 generation of flood waves (Richie et al., 1989), the liberation of solutes and nutrients from soil and  
41 sediment (Gaillardet et al., 1999; Jin et al., 2010), the physical breakdown of sediment in streams (Attal and  
42 Lave, 2006), and the decomposition of organic matter (Taylor and Chauvet, 2014). Thus travel distance is  
43 another fundamental aspect of the link between source and outlet for water, solutes, sediment, and  
44 nutrients.

45 Together, the effects of elevation and travel distance should govern the amount, timing, and  
46 composition of fluxes from catchments. However, previous work has explored the distributions of elevation  
47 and travel distance separately, without consideration of their joint distribution. The distribution of  
48 elevations – known as hypsometry – reveals the vertical structure of a catchment and has been used to  
49 quantify landscape development, identify geomorphic process regimes, and understand the sensitivity of  
50 land area to changes in sea level (Strahler, 1952; Lifton and Chase, 1992; Brozovic et al., 1997;  
51 Brocklehurst and Whipple, 2004; Algeo and Soslavinsky, 1995). Meanwhile, the distribution of travel  
52 distances – known as the width or area function – reveals the horizontal structure of catchments and has  
53 been used to characterize catchment shape, identify channel branching structure, and understand  
54 hydrographs (Gupta and Mesa, 1988; Rinaldo et al., 1995; Sklar et al., 2006; Moussa, 2008; Rigon et al.,  
55 2015).

56 Although both the hypsometry and width functions of catchments have been widely studied, to our  
57 knowledge elevation and travel distance have only been considered together in an analysis of the  
58 hypsometry of channel network links (Gupta and Waymire, 1989) and in plots of longitudinal profiles of  
59 trunk streams and tributaries (Rigon et al., 1994). Thus, previous research has overlooked the insights that  
60 might be gained by analyzing hillslopes and channels together as a collection of paired values of elevation  
61 and travel distance. Some questions that might be addressed by such an analysis include: Which if any  
62 aspects of the joint distribution of elevation and travel distance are common from one catchment to the  
63 next? What are the most revealing measures of differences in the distributions across different catchments?  
64 Do the distributions differ in ways that systematically reflect the factors that drive landscape evolution,  
65 such as weathering, climate, and tectonics?

66 Here we address these questions using topographic data from three catchments of differing area  
67 and relief. First we explore how the distributions of elevation and travel distance vary across our study  
68 catchments. Then we show how elevation and travel distance can be combined into a single quantity,  
69 referred to here as catchment power because it expresses the rate of potential energy dissipation of water  
70 and sediment as they travel down slopes. Next, using our analyses of the elevation and travel distance  
71 distributions from the study catchments, we develop an approach for generating synthetic catchments that



72 capture many features of power distributions in natural landscapes and thus can be used to explore how  
73 factors such as area, relief, and profile concavity influence catchment power. Finally, we discuss how our  
74 approach provides a new framework for understanding how rivers are influenced by upstream sources of  
75 water, solutes, and sediment in catchments.

## 76 **2. Elevation and travel distance in natural landscapes**

77 To explore how joint distributions of elevation and travel distance vary in natural landscapes, we  
78 chose catchments drained by Inyo Creek, Providence Creek, and the Noyo River, all in California, USA  
79 (Fig. 1). Each of these catchments has been featured in previous studies of the production and delivery of  
80 water, solutes, and sediment from slopes to channels. Thus our selection of sites allows us to link analyses  
81 of elevation and travel distance distributions to existing research on physical, chemical, and biological  
82 processes in the catchments. All of the catchments are developed in mountain landscapes, where the  
83 products of runoff, weathering, and erosion reach the outlet without any long-term interception in  
84 floodplains or lakes; thus, the travel distance distributions should strongly reflect transport processes in the  
85 catchments. At each site, we extracted elevations from a 10-m digital elevation model (DEM) and  
86 calculated travel distance to the outlet using a steepest descent algorithm (Tarbotton, 1997). The  
87 catchments span a range in relief, drainage area, and mean slope (Table 1), and thus also a range in the  
88 populations of paired values of elevation and travel distance (Fig. 1).

### 89 **2.1 Study sites**

90 The Inyo Creek catchment spans 2 km of relief over 4 km of travel distance on the eastern slope of  
91 the High Sierra (Table 1). Unlike some of its neighboring catchments along the range, it has never been  
92 scoured by glaciers, making it ideal for comparison of sediment production and landscape evolution in  
93 glaciated and non-glaciated terrain (Riebe et al., 2015; Stock et al., 2006; Brocklehurst and Whipple, 2002).  
94 Moreover, the catchment spans a range in the relative importance of physical, chemical, and biological  
95 weathering from its warm, gently sloped, low elevations to its cold, steep headwaters.  
96 On the other side of the Sierra Nevada, Providence Creek spans 1 km of relief over 8 km of travel  
97 distance (Table 1). This catchment is part of the Southern Sierra Critical Zone Observatory, which has been  
98 the focus of numerous recent studies of hydrology, biogeochemistry, and geomorphology (e.g., Bales et al.,  
99 2011; Hunsaker and Neary, 2012; Hunsaker et al., 2012; Goulden and Bales, 2014; Holbrook et al., 2014;  
100 Hahm et al., 2014). Precipitation in the upper half of the catchment dominantly falls as snow, whereas  
101 precipitation in the lower half dominantly falls as rain. Unlike the roughly continuous concave ridge and  
102 channel profiles of Inyo Creek, catchment topography in Providence Creek exhibits a pronounced step in  
103 elevation of both the channel and ridge profiles (Fig. 1). Steps like these, which are common on the  
104 southwestern slope of the Sierra Nevada, have been interpreted to reflect a feedback between weathering  
105 and erosion (Wahrhaftig, 1965).



106 Farther to the northwest, in the California Coast Ranges, the Noyo River catchment spans 0.9 km  
107 of relief over 20 km of travel distance. Thus the catchment is significantly larger and more gently sloped on  
108 average than either of the other two study catchments. The catchment has a long history of intensive timber  
109 harvests and has been the site of numerous studies of the effects of land use on in-stream habitat (Burns,  
110 1972; Lisle, 1982; Leithold et al., 2006; ) and the role of topography and channel network structure in the  
111 production and delivery of sediment from slopes to channels (Dai et al., 2004; Sklar et al., 2006).

## 112 2.2 Spatial distributions of elevation and travel distance

113 The maps in Figure 2 show the spatial distributions of elevation and travel distance across each  
114 catchment. Broadly, travel distance and elevation covary in space; the highest elevations in each catchment  
115 tend to be further away from the outlet. However, in detail, elevation contours are not aligned with contours  
116 of equal travel distance; in general the elevation contours exhibit higher planform curvature than travel  
117 distance contours. Thus, for a given elevation contour, travel distances are longest in the valley axis and  
118 shortest at the ridges. Conversely, for a given travel distance, elevations are highest at the ridges and lowest  
119 in the valley axis. These patterns are especially clear at Inyo Creek (Fig. 2a) and Providence Creek (Fig.  
120 2b), which drain small, relatively undissected catchments.

121 The patterns in elevation and travel distance in the Noyo River catchment are more complex (Fig.  
122 2c), in part because it is more deeply incised by multiple high-order trunk streams. At ridges that separate  
123 these trunk streams, travel distance can vary considerably from one side of the ridge to the other. Thus  
124 nearby points that share the same elevation can have very different travel distances. For example, along the  
125 central ridge, which runs along the catchment's axis, points on the south side of the ridge drain to a more  
126 sinuous and thus longer southern trunk stream, giving them longer travel distances to the outlet than points  
127 on the northern side. For the same travel distance, points occur at higher elevations in the northern, less  
128 sinuous trunk stream.

## 129 2.3 Hypsometry and the width function

130 The spatial patterns shown in the maps are reflected in both the hypsometry and the width  
131 function, which are the conventional ways of displaying distributions of elevation and travel distance  
132 separately (Fig. 3). For example, hypsometry shows that most of the Inyo Creek catchment occurs at mid  
133 elevations (Fig. 3a), because the catchment narrows both at low elevation near the outlet and at high  
134 elevation near the catchment divide (Fig. 2a). This differs from the hypsometry of Providence Creek, where  
135 most of the catchment area occurs at higher elevations, above the pronounced step in the topography.  
136 Meanwhile, at the Noyo River site, the majority of area occurs at lower elevations, because the catchment  
137 is deeply dissected, with wide valley bottoms and steep, narrow ridges.

138 Hypsometry reveals differences in the vertical structure of the catchments, whereas the width  
139 function reveals differences in planform structure, which are governed in part by differences in the shapes





140 of the catchment boundaries. For example, the distribution of travel distances at Inyo Creek is symmetrical,  
141 reflecting the roughly oval shape of the catchment. Meanwhile, at Providence Creek, the distribution of  
142 travel distances is bimodal, reflecting the narrowing near the middle of the catchment. At the Noyo River  
143 site, the travel-distance distribution is skewed, with the majority of the area at long travel distances,  
144 reflecting the widening of the catchment with increasing distance from the outlet that is evident in Figure  
145 2c.

#### 146 **2.4 Joint distributions of elevation and travel distance**

147 Figure 3 shows that much can be learned from the distributions of elevation and travel distance  
148 plotted alone. However, they do not reveal information contained in the distribution of paired values of  
149 elevation and travel distance. One particularly insightful index that can be missed is the ratio of elevation to  
150 travel distance, which is the mean slope for water, solutes, and sediment on a path of steepest descent from  
151 source to outlet. The ranges in elevations and travel distances from these three catchments imply that the  
152 distribution of mean slopes differ markedly across our sites (Table 1; Fig. 1). These differences likely  
153 correspond to differences in factors such as water-transit times, sediment breakdown rates, and channel  
154 morphology. Although information on the distribution of mean slopes is embedded in both the hypsometry  
155 and the width function, it cannot be extracted from either of them plotted alone or even plotted side by side  
156 (Fig. 3).

157 To overcome the limitations of separate plots of vertical and horizontal structure, we plotted the  
158 joint distribution of elevation and travel distance for every point in each of the catchments in Figure 4.  
159 These plots show both the long profile of the channel network and the distribution of hillslope sources,  
160 which account for more than 98% of the source area in each catchment. A number of similarities emerge  
161 across the sites (Fig. 4a-c). Strikingly, at the highest elevations for any given travel distance, sources are  
162 aligned in steeply-sloped tendrils of data that coalesce at lower elevations. These tendrils represent hillslope  
163 sources aligned along common flow paths that cluster together into narrow groups. Equally striking are the  
164 gaps between the tendrils, which represent paired values of elevation and travel distance that do not occur  
165 anywhere in the catchment. Meanwhile, some paired values are so common that they overlap, particularly  
166 along flowpaths that converge near the mainstem channel. Thus the joint distribution plots generally show  
167 dense concentrations of data points at low elevations for any given travel distance.

168 Bivariate frequency distributions help shed light on the degree of clustering and overlap of data at  
169 shared values (Fig. 4 d-f). These binned representations of the raw data show that, for a given travel  
170 distance, as elevation decreases, data point density generally increases to a peak and then quickly tapers to  
171 zero. They also show that the density of paired values is highest at 60 and 80% of the maximum travel  
172 distance, with a tapering in point density at both the upstream and downstream ends of the catchment.

173 Although the joint distributions are similar in some respects across the catchments, they also  
174 exhibit significant differences that cannot be inferred from the conventional representations of vertical and  
175 horizontal catchment structure in Fig. 3. For example, the relative slopes of the tendrils and the channels



176 differ markedly. The tendrils are much steeper than the mainstem channel profile in the Noyo River  
177 catchment (Fig. 4f). Conversely, in the other two catchments, the tendrils and the main channel profile have  
178 similar slopes, especially at Providence Creek. These differences likely arise at least in part due to the  
179 difference in scale of the watersheds; in the Noyo River catchment, some of the individual tendrils  
180 encompass large areas, similar in scale to the entire Inyo and Providence Creek catchments. Thus we  
181 interpret the tendrils along the Noyo River to be tributary catchments that are similar to the Inyo and  
182 Providence Creek catchments, with tendrils of their own that are only slightly steeper than the local  
183 tributary channel slopes.

184 Perhaps the most striking difference among the catchments can be seen in the distributions of  
185 mean slope along the travel path to the outlet, which we calculate as the ratio of the paired values of  
186 elevation and travel distance (Fig. 5a-c insets). Swaths of common mean slope appear as linear trends  
187 through the joint distributions of elevation and travel distance (Fig. 5a-c), or as contours on a planform  
188 view of the catchment (Fig. 5d-f). In each catchment the contours of mean slope (Fig. 5d-f) differ markedly  
189 from the contours of elevation and travel distance (Fig. 2). Mean slopes are relatively steep and span a  
190 relatively narrow range at Inyo Creek (Fig. 5c) compared to the Noyo River catchment (Fig. 5f).  
191 Providence Creek is distinguished by a peak in mean slopes (Fig. 5b) corresponding to the upper half of  
192 catchment, above the step in the topography (Fig. 5e).

193 Mean slope quantifies the ratio between elevation and travel distance, and thus is a single metric  
194 that combines two fundamental attributes of source areas in catchments. The distributions of source  
195 elevation, travel distance, and thus mean slope are ultimately set by the erosion and transport processes that  
196 produce and deliver sediment from slopes to channels. Thus spatial variations in mean slope, such as those  
197 shown in Fig. 5, may be closely linked to spatial variations in the production and delivery of water, solutes,  
198 and sediment.

### 199 **3 Source-area and catchment power**

200 To develop a mechanistic framework for linking distributions of source-area mean slope with  
201 catchment processes, we introduce the concept of source-area power, which integrates elevation, travel  
202 distance, and the production rate of material on slopes. In the derivation that follows, we consider a mass  
203 ( $M$ ) of transportable material (such as water, solutes, or sediment) produced at a source elevation  $z$  on a  
204 hillslope and delivered downstream to an elevation  $z_o$  at the catchment outlet. The potential energy ( $E$ ) of  
205 the material at the source, relative to the outlet is given by Equation 1:

$$206 \quad E_{i,j} = M_{i,j} g R_i = \rho_{i,j} A_i h_{i,j} g (z_i - z_o) \quad (1).$$

207 Here  $g$  is acceleration due to gravity,  $R$  is relief (i.e., the difference in elevation between the source and  
208 outlet),  $\rho$  is density,  $h$  is the thickness of the material produced at the source,  $A$  is the area of the source  
209 (one pixel in a DEM), the subscript  $i$  refers to the specific source location on the slope, and the subscript  $j$



210 refers to the type of material (i.e., water, solutes, or sediment). In the case of solutes,  $h$  refers to the  
211 equivalent thickness of chemical erosion needed to account for the mass loss due to production of solutes.  
212 At each source, potential energy is produced at a rate ( $\Omega$ ) that is proportional to the production  
213 rate ( $Q$ ) or flux of material from the source, as shown in Equation 2:

$$214 \quad \Omega_{i,j} = Q_{i,j} g R_i = \rho_{i,j} A_i \frac{\partial h_{i,j}}{\partial t} g (z_i - z_o) \quad (2).$$

215 Here, the definition of  $\partial h/\partial t$  (in dimensions of length per time) depends on the process considered. For  
216 water produced by precipitation,  $\partial h/\partial t$  is the precipitation rate. For sediment produced by erosion,  $\partial h/\partial t$  is  
217 the physical erosion rate. For solutes produced by chemical erosion,  $\partial h/\partial t$  is the equivalent to the chemical  
218 erosion rate. In all cases,  $\Omega$  has dimensions of power.

219 On its journey to the outlet, the material loses its potential energy. This energy is converted to  
220 kinetic energy and is primarily lost to heat due to friction. In the case of sediment, some of the energy is  
221 consumed when particles are abraded and shattered during collisions with other particles and the channel  
222 bed. Thus it may be useful in the context of geomorphic work to think of the power expended by the water  
223 or sediment over the travel distance ( $L$ ) between the source and outlet, as shown in Equation 3:

$$224 \quad \omega_{i,j} = \frac{Q_{i,j} g R_i}{L_i} = \rho_{i,j} A_i \frac{\partial h_{i,j}}{\partial t} g \frac{(z_i - z_o)}{L_i} \quad (3).$$

225 Here  $\omega$  is the source-area power, which has dimensions of power per length, and  $(z_i - z_o)/L_i$  is the mean slope  
226 along the travel path from the source to outlet. The concept of source-area power allows us to explore the  
227 possible implications of variability in the ratio of elevation to travel distance (i.e., the mean slope) on the  
228 production and delivery of water, solutes, and sediment across catchments.

229 For example, in landscapes where the rate of precipitation or erosion is spatially uniform, we  
230 expect the distribution of source-area power for the water or sediment to be identical to the distribution of  
231 the mean slopes of source areas. In contrast, in landscapes where rates of precipitation and erosion are  
232 spatially variable and sometimes correlated (Reiners et al., 2003; Burbank et al. 2003), we expect the  
233 distributions of power and mean slopes to differ. This is the case at Inyo Creek where mean annual  
234 precipitation increases with elevation from 290 mm yr<sup>-1</sup> at the outlet to 710 mm yr<sup>-1</sup> at the catchment divide  
235 (Prism Climate Group, 2014), and the rate of production of sediment by erosion has been estimated to  
236 increase exponentially with elevation from 0.03 mm yr<sup>-1</sup> at the outlet to 1.5 mm yr<sup>-1</sup> at the divide (Riebe et  
237 al., 2015). When we combine these relationships for water and sediment production with the distribution of  
238 mean slopes using Equation 3, we arrive at maps showing the spatial distributions of source-area power for  
239 the two materials, water and sediment (Fig. 6a-b). In both cases, the power contours are stretched towards  
240 the catchment divide, relative to the case of uniform precipitation and erosion (equivalent to Fig. 5a),  
241 especially in the case of spatially varying erosion (Fig. 6b), due to the nonlinear relationship between  
242 erosion rate and elevation.



243 Because the altitudinal gradients in erosion and precipitation are known, we can use them to  
 244 explore how the source-area power of water varies across the catchment, relative to the amount of sediment  
 245 that must be produced on hillslopes and transported to the outlet, assuming steady state. We define a  
 246 dimensionless ratio ( $\omega_{w,s}^*$ ) that quantifies the source-area power of water per mass of sediment eroded at  
 247 an individual pixel,  $i$ :

$$248 \quad \omega_{w,s}^* = \frac{\omega_{i,w}}{gQ_{i,s}} = \frac{\rho_w (\partial h_{i,w} / \partial t) (z_i - z_o)}{\rho_s (\partial h_{i,s} / \partial t) L_i} \quad (4)$$

249 Here the subscript  $w$  refers to water produced from precipitation, and the subscript  $s$  refers to sediment  
 250 produced from erosion. The spatial distribution of  $\omega_{w,s}^*$  shows that the relative amount of water power  
 251 available to produce and transport sediment increases from 36 to 653 (mean  $\pm$  standard deviation =  
 252  $254 \pm 149$ ) from the headwaters to the catchment mouth (Fig. 6C). We interpret this factor of 18 change to  
 253 reflect shifts from headwaters to outlet in dominant geomorphic processes. For example, on headwater  
 254 slopes where less water is available and  $\omega_{w,s}^*$  is lowest, we might expect that sediment transport is  
 255 dominated by gravity-driven mass wasting and that weathering is dominated by physical rather than  
 256 chemical processes. In contrast, on slopes near the catchment mouth, where  $\omega_{w,s}^*$  is highest, we might  
 257 expect that sediment transport is dominated by water-driven erosion (e.g., via sheetwash and channelized  
 258 flow), and that weathering is dominated by chemical processes. This is broadly consistent with field  
 259 observations: headwater slopes consist of steep, landslide-dominated bare bedrock, whereas slopes near the  
 260 catchment outlet are gentler, more vegetated, and soil mantled, implying that chemical weathering is  
 261 favored by longer residence times of water and sediment (Riebe et al., 2015).

262 To characterize power at the scale of whole catchments, we sum Equation 3 over the entire  
 263 contributing area, using Equation 5

$$264 \quad \omega_{c,j} = g \sum_{i=1}^{i=N} \rho_{i,j} A_i \frac{\partial h_{i,j}}{\partial t} \frac{(z_i - z_o)}{L_i} \quad (5).$$

265 Here  $\omega_{c,j}$  is the catchment-integrated source-area power for the material of interest  $j$ , or, more simply,  
 266 “catchment power.” It expresses the total power expended as the potential energy of material produced  
 267 throughout the catchment is lost along flow paths to the outlet. For Inyo Creek, the total catchment power  
 268 for water is  $166 \text{ W m}^{-1}$ , while the total catchment power for sediment is  $0.122 \text{ W m}^{-1}$ . The ratio of  
 269 catchment power for water to sediment is 136. This ratio reflects the combined effects of the steep  
 270 altitudinal increase in erosion rates, the more modest altitudinal increase in precipitation rates, and how  
 271 these trends map into the joint distribution of elevation and travel distance.

272 New theory and data from other landscapes are needed to interpret spatial variations in power  
 273 across individual catchments and to understand why they vary from catchment to catchment. For example,



274 we might expect to find a different spatial distribution of water-sediment power ratios, relative to Inyo  
275 Creek, in a catchment with a different hypsometry and width function. Likewise, the spatial distribution of  
276 source-area power would differ greatly in a catchment responding to accelerated base-level lowering, with  
277 faster erosion rates near the outlet. Moreover, we might expect the ratio of water to sediment catchment  
278 power to vary considerably from catchment to catchment across gradients in climate and tectonics.  
279 Understanding these variations could provide fresh insights into the geomorphic processes that shape  
280 landscapes.

281 Although our analysis of power at Inyo Creek focused on the production of water and sediment, it  
282 can be extended to any material that varies in production rate with altitude or varies in delivery to the outlet  
283 as a function of travel distance. For example, production rates of solutes, nutrients, contaminants, and even  
284 cosmogenic nuclides could be substituted for the production rate terms in Equations 2-5. Thus it should be  
285 possible to use the new frameworks of source-area and catchment power to model, and thus better  
286 understand, both the spatial distribution and catchment-integrated effects of geomorphic, geochemical, and  
287 ecosystem processes.

288 Our analysis of Inyo Creek shows how the power framework can be applied to natural landscapes  
289 using a DEM. However, factors, such as climate, topography, and tectonics, which might influence power  
290 and thus merit further investigation, are closely coupled together. This makes it difficult to isolate any  
291 single factor of interest in comparisons of power across catchments. Moreover, some catchments, such as  
292 Providence Creek, have peculiarities in shape and structure that dominate patterns of power (Fig. 5b) and  
293 thus might confound comparisons of one catchment to the next. To overcome the limitations of using  
294 DEMs from individual catchments, we developed an approach that generates synthetic catchments based on  
295 scaling relationships for catchment geometry and topography. Thus we can systematically explore how  
296 variations in factors such as area, relief, and profile concavity influence the distribution of source-area and  
297 catchment power in landscapes. In the next section we show that our synthetic catchments capture the  
298 fundamental characteristics of the joint distribution of elevation and travel distance in landscapes. Thus we  
299 can use them to isolate and thus study the influence of physical, chemical and biological factors that govern  
300 catchment processes.

#### 301 **4 Synthetic joint distributions of elevation and travel distance**

302 Our goal in developing synthetic catchments is to generate realistic joint distributions of elevation  
303 and travel distance (e.g., that are comparable to those shown in Fig. 3). Equations 3-5 show that this should  
304 be sufficient to quantify distributions of source-area and catchment power. Hence there is no need for a  
305 spatially explicit representation of topography, because calculating source-area power does not require  
306 information about spatial position of channels or topographic factors such as hillslope gradient or curvature.  
307 Populating the joint distribution of elevation and travel distance only requires specifying the upper and  
308 lower boundaries at each travel distance and then distributing area across elevations in the space between  
309 the boundaries. Although theory is available to generate main-stem longitudinal profiles that could serve as



310 a realistic lower boundary of the distribution, we are unaware of any theory for predicting ridge profiles  
311 and thus delineating a realistic upper boundary. Most importantly, to our knowledge, no theory is available  
312 for populating the elevation distribution for a given travel distance between the upper and lower  
313 boundaries, without creating a spatially explicit synthetic DEM using a landscape evolution model  
314 (Coulthard, 2001; Willgoose, 2005; Tucker and Hancock, 2010).

315 As a starting point for overcoming these limitations, we adopt a statistical, empirical approach,  
316 using Inyo Creek as a prototype for a relatively simple, symmetrical low-order catchment. We start with the  
317 actual maximum and minimum elevations at each travel distance and use a statistical optimization  
318 procedure to find the best-fit distribution of elevations. We then develop expressions for the upper and  
319 lower boundaries at each travel distance and use the best-fit area-versus-elevation function to define a fully  
320 synthetic joint distribution of elevation and travel distance.

#### 321 4.1 Area-versus-elevation at each travel distance

322 To find the best-fit relationship between area and elevation at each travel distance, we parsed the  
323 Inyo Creek catchment into forty-seven 100-m wide travel distance bins (Fig. 7A). Figure 7B shows  
324 distributions of area with elevation for seven representative travel distance bins. Inspection of figure 7B  
325 suggests that the area under the curves scales with local relief (i.e., the width across the base of the curve),  
326 and that the distributions are consistently right skewed, with more area at the lower elevations. When we  
327 sum area and relief across all bins, and plot the fractional area versus fractional relief for each bin, we find  
328 that the data roughly follow a 1:1 line (Fig. 7C). We obtain a similar result for a variety of bin spacings,  
329 which suggests that the area-elevation relationship is self similar: when the upper and lower boundaries are  
330 farther apart (i.e., when local relief is higher), the area contained within the travel distance bin increases in  
331 direct proportion to the difference in relief. This permits a collapse of the distributions of elevation for each  
332 travel distance bin, by normalizing elevation with local relief, and area by total area in the bin. Figure 7D  
333 shows the normalized hypsometry for travel distance bins spanning the entire Inyo Creek catchment. The  
334 broad consistency of the shapes of the normalized distributions suggests that a single functional form could  
335 represent the central tendency, spread and even the skew of the distribution of area with elevation for any  
336 travel distance across the catchment.

337 The beta distribution has a simple functional form that captures two key characteristics of the  
338 normalized area-elevation relationships: it is bounded by 0 and 1, and it can have right-skew depending on  
339 the values of its two shape factors,  $\alpha$  and  $\beta$ . Thus a beta distribution is well suited to generating synthetic  
340 distributions of area as a function of elevation.

341 A generic form of the beta distribution is shown in Equation 6

$$342 \quad f_{\beta} = x^{\alpha-1} (1-x)^{\beta-1} \quad (6).$$



343 Here  $f_\beta$  is the height of the beta distribution at point  $x$ , where  $x$  ranges from 0 to 1 and the sum of area under  
 344 the curve is equal to 1.

345 To find the values of  $\alpha$  and  $\beta$  that correspond to the best fit between the area-elevation data and  
 346 the beta distribution across all travel distances at Inyo Creek, we first converted Equation 6 to Equation 7  
 347 for dimensional consistency.

$$348 \quad f_{A(z,L)} = A_L (z^*)^{\alpha-1} (1 - z^*)^{\beta-1} \quad (7).$$

349 Here,  $f_{A(z,L)}$  is the height of the scaled beta distribution at elevation  $z$  in travel distance bin  $L$ ,  $A_L$  is the area  
 350 in the travel distance bin, and  $z^* = (z - z_C) / (z_R - z_C)$  where  $z_C$  is the elevation of the channel, and  $z_R$  is  
 351 the elevation of the ridge.

352 By applying Equation 7 to each travel distance bin, we can generate a synthetic joint distribution  
 353 of elevation and travel distance. We then can calculate the misfit between the synthetic and actual joint  
 354 distributions as the square root of the mean squared differences (RMSE) at each elevation and travel  
 355 distance. To find the best-fit parameters, we used an optimization algorithm to search for the pair of shape  
 356 factors that minimize the misfit. For Inyo Creek data, with 100 m travel distance bins, and 40 m elevation  
 357 bins (Fig. 7), the best-fit  $\alpha$  is 2.6 and best-fit  $\beta$  is 3.4. The objective function for this case is shown in  
 358 Figure 8. The best-fit parameters yield a beta distribution that follows the trend in the normalized area  
 359 distributions shown in Figure 7D.

360 To quantify the model performance, we use the Nash-Sutcliffe model efficiency statistic ( $NS$ )  
 361 (Nash and Sutcliffe, 1970), which is calculated as

$$362 \quad NS = 1 - \frac{\sum (f_{A-Model} - f_{A-Data})^2}{\sum (f_{A-Mean} - f_{A-Data})^2} \quad (8).$$

363 Here the subscript ‘model’ refers to the predictions of Equation 7, ‘data’ refers to the DEM, and ‘mean’  
 364 represents a uniform area density in each bin equal to the total area divided by the number of distance and  
 365 elevation bins containing data. A model efficiency of 1 implies a perfect match between predictions and  
 366 observations. An efficiency of 0 indicates that model predictions are only as accurate as simply using the  
 367 mean of the observed data. Less than zero efficiency ( $NS < 0$ ) implies that the observed mean is a better  
 368 predictor than the model. In other words, the closer the model efficiency is to 1, the more accurate the  
 369 model is. For this particular binning scheme (100 m distance and 40 m elevation bins), the Nash-Sutcliffe  
 370 model efficiency statistic for Inyo Creek is 0.41, indicating good but not excellent agreement with the  
 371 topographic data.

372 To explore the sensitivity of model performance to spatial resolution of the binning scheme, we  
 373 repeated the optimization procedure described above for a range of travel distance and elevation bin sizes.  
 374 As shown in Figure 9A, the  $NS$  values are generally higher for larger bin sizes (i.e. fewer bins), reaching a  
 375 local maximum ( $NS > 0.7$ ) for 400 m travel distance bins. Model efficiency approaches 1.0 ( $NS > 0.9$ ) for a





376 single distance bin, which is equivalent to fitting the whole catchment hypsometry with a single beta  
 377 distribution curve. The best-fit values of the beta distribution shape parameters vary considerably with the  
 378 size of the distance and elevation bins, and are highly correlated (Fig. 9B); the range of resulting  
 379 distribution shapes are illustrated in Figure 9C.

380 These results reveal a tradeoff between model performance and spatial resolution. They also  
 381 suggest that, to first order, Equation 7 can capture much of the structure of area as a function of relief at  
 382 Inyo Creek. To the extent that we can think of Inyo Creek as a prototypical catchment, we can use Equation  
 383 7 to generate synthetic joint distributions of elevation and travel distance for other catchments, with  
 384 different channel and ridge profiles.

385 The good fit between the modeled and observed joint distributions of elevation and travel distance  
 386 at Inyo Creek arises in part because the actual profiles of the channel and ridge were used as envelopes on  
 387 the area-elevation distributions. This ensures that the boundaries of the modeled joint distribution  
 388 correspond to actual topographic data. To generate a fully-synthetic joint distribution of elevation and  
 389 travel distance, an approach is needed that not only distributes area across elevations but also produces  
 390 synthetic channel and ridge profiles that define the upper and lower boundaries of elevation as a function of  
 391 travel distance.

## 392 4.2 Main-stem channel and ridge profiles

393 For any travel distance, the lowest elevation will be on the channel main-stem. Thus, the main-  
 394 stem long profile is the lower boundary for the joint distribution of elevation and travel distance. Channel  
 395 elevations ( $z_C$ ) are commonly modeled as a power function of travel distance ( $x$ ) along the main stem from  
 396 the outlet to the upstream limit of fluvial processes (i.e., the distance to the “channel head”, denoted  $x_{ch}$ ). As  
 397 elaborated in the appendix, here we derive an expression for channel elevation that extends all the way to  
 398 the top of the catchment, at the point where the valley axis meets the drainage divide.

399 From the outlet to  $x_{ch}$ , the elevation of the channel can be written as:

$$400 \quad z_C = k_C \left[ \left( L_{max} \right)^{1-\theta H} - \left( L_{max} - x \right)^{1-\theta H} \right] \text{ for } 0 \leq x \leq x_{ch} \quad (9a).$$

401 Here,  $L_{max}$  is the travel distance to the outlet from the furthest point in the catchment,  $\theta$  and  $H$  are the  
 402 exponents in Flint’s Law and Hack’s Law respectively, and  $k_C$  is a constant that lumps together  $\theta$ ,  $H$  and  
 403 other factors, as shown in the appendix.

404 For the valley axis upstream of the channel head, from  $x_{ch}$  to  $L_{max}$ , the elevation profile can be  
 405 written as follows (see appendix for derivation):

$$406 \quad z_C = k_C \left[ \left( L_{max} \right)^{1-\theta H} - \left( L_{ch} \right)^{1-\theta H} \right] + S_h \left( x - x_{ch} \right) \quad \text{for } x_{ch} < x \leq L_{max} \quad (9b)$$



407 Here,  $L_{ch}$  is the distance from the channel head to the outlet and  $S_h$  represents a uniform slope over the  
408 distance between  $L_{ch}$  and  $L_{max}$ .

409 The upper boundary of the joint distribution of elevation and travel distance is defined by the  
410 collection of points at the highest elevations in each travel distance bin. Unlike the channel profile, which  
411 defines the base of the joint distribution, the points at the upper boundary do not necessarily lie along a  
412 contiguous path. Nevertheless, for simplicity we refer to these points as the ridge profile, and assume that  
413 its elevation follows a simple power-law relationship with distance.

$$414 \quad z_R = k_R x^P \quad (10)$$

415 Here  $k_R$  is an adjustable parameter and the exponent  $P$  depends on the parameters of the channel profile. As  
416 elaborated in the appendix, we impose the constraints that the ridge profile intersects the main-stem  
417 channel profile at the two end points, where  $x = 0$  and  $x = L_{max}$ , in order to define the parameter  $P$ .

### 418 4.3 Scaling between area and relief

419 Equations 9 and 10 provide the values of  $z_C$  and  $z_R$  that are needed in Equation 7 to define the local  
420 relief for any travel distance. However, before Equation 7 can be used to generate synthetic distributions of  
421 elevation and travel distance, the area in each travel distance bin ( $A_L$ ) must be defined. We do so using the  
422 previously discussed self-similar relationship between area and local relief shown in Figure 7C, where the  
423 fraction of the total area in a travel bin of interest is proportional to the local relief divided by the sum of  
424 local relief over all travel distance bins. For Inyo Creek, this relationship holds for any choice of bin  
425 spacing and it is expressed mathematically in Equation 11

$$426 \quad \frac{A_L}{A_C} = \frac{A_L}{\sum_{L=1}^N A_L} = \frac{R_L}{\sum_{L=1}^N R_L} \quad (11).$$

427 Here,  $N$  is the number of bins,  $A_C$  is the catchment area, which is equal to the sum of all  $A_L$ , and  $R_L$  is the  
428 relief in the travel distance bin, which is equal to  $z_R - z_C$ . Following Hack's Law, the total area of the  
429 catchment ( $A_C$ ) can be treated as a power function of  $L_{max}$  (see appendix).

### 430 4.4 Generating synthetic distributions of elevation and travel distance

431 Equations 7, 9, 10 and 11 can be used to generate fully synthetic distributions of elevation and  
432 travel distance that are coupled to fundamental scaling relationships of natural catchments (expressed in  
433 Hack's and Flint's laws). Moreover, this permits us to tune parameter values to reproduce catchments of  
434 specific sizes and shapes. For example, Figure 10 shows the synthetic joint distribution of elevation and  
435 travel distance for a catchment with size and shape similar to Inyo Creek (see appendix for the list of model  
436 parameters used to generate this plot). By projecting the joint distribution of elevation and travel distance



437 onto the two orthogonal axes, we obtain the hypsometric curve and width function for the synthetic  
438 catchment (Fig. 10, panels B and C). Thus, although the hypsometry and width function cannot be used  
439 alone or together to generate the joint distribution of elevation and travel distance, they can be derived from  
440 it. Nash-Sutcliffe statistics calculated from a comparison of the fully synthetic (Fig. 10A) and true  
441 distribution (Fig. 4D) vary with bin size as in the previous case using the actual channel and ridge profiles,  
442 as shown in Figure 9. However, NS values for a given binning scheme are generally lower. This result  
443 suggests that the fully synthetic formulation is less efficient than the partly synthetic formulation of section  
444 4.1 at explaining variance in the joint distribution of elevation and travel distance. This loss of efficiency  
445 arises due to error in fitting the upper and lower boundaries with the channel and ridge profile curves of  
446 Equations 9 and 10.

## 447 5. Discussion

### 448 5.1 Extending the model to other catchments

449 The fully synthetic formulation for the joint distribution of elevation and travel distance was  
450 calibrated using data from Inyo Creek, under the assumption that it is a prototypical catchment. But Inyo  
451 Creek is relatively small and steep. This raises the question of whether the synthetic formulation yields  
452 realistic results in other landscapes with lower relief or higher area.

453 Our other two study catchments, Providence Creek and Noyo River have lower relief and greater  
454 area, respectively (Fig. 1). Hence we can use them to gauge the performance of the synthetic formulation  
455 across a range of conditions. First we evaluated how well the beta distribution can be used as a predictor of  
456 the distribution of elevation at each travel distance. Results are shown in Figure 11, which displays  
457 normalized area-versus-elevation distributions for Providence Creek and Noyo River together with the  
458 best-fit beta distributions for each catchment (with travel distance and elevation binned at 1/20 of  
459 maximum values). The central tendency, spread, and skew of the best-fit beta distributions all appear to  
460 roughly follow the patterns exhibited in the data. However, the values of the best-fit shape parameters  
461 differ between these two catchments, as well as with Inyo Creek for this binning scheme. This suggest that  
462 the joint distribution of travel distance and elevation, as represented by these model parameters, may differ  
463 systematically between catchments.

464 The three catchments we analyzed vary across gradients in relief and drainage area (Fig. 1), but  
465 also in the degree of dissection and channel profile shape, which may in turn reflect differing lithologic,  
466 tectonic or climatic boundary conditions. For example, Providence Creek has a pronounced step in the  
467 channel profile, with greater local relief and area concentrated in the upper part of the catchment (Fig. 2).  
468 This step may arise due to feedbacks between weathering of biotite and topographic slope across the  
469 landscape (Wahrhaftig, 1965). As a result, the channel profile is not well-fit by a power equation or any  
470 other simple function. In contrast, the larger Noyo River catchment has a smooth, highly concave main-



471 stem channel profile, and greater area at longer travel distances to the outlet due to a high degree of channel  
472 branching. The Noyo River main-stem channel profile may be influenced by aggradation due to sea-level  
473 rise, and is better represented in the fully synthetic model using an exponential equation instead of a power  
474 equation (see appendix).

475 Another second way to gauge model performance for various catchments is to compare predicted  
476 hypsometric curves and width functions using the projections of the modeled and measured joint  
477 distributions onto the elevation and travel distance axes, as we did in Fig. 10 for the fully synthetic Inyo  
478 Creek case. Figure 11 shows hypsometric curves and width functions for the three study catchments  
479 generated with the DEM data ('actual'), the partially-synthetic formulation using actual profiles and  
480 modeled area distributions (Eqns. 7 and 11), and the fully-synthetic formulation using modeled profiles.  
481 For Inyo Creek, both the partly and fully synthetic models provide good fits to the overall shape of the  
482 actual hypsometry and width function (Fig. 11a-b). In contrast, at Providence Creek, the partly synthetic  
483 model only captures the hypsometry and width function over portions of the distributions, and performs  
484 particularly poorly in the wide upper part of the catchment (Fig. 11c-d). Meanwhile, the fully synthetic  
485 model performs more poorly because the modeled channel profile fails to capture the step in the  
486 topography (Fig. 11 c-d). At Noyo River, despite its larger area, both the partly and fully synthetic models  
487 perform reasonably well over all elevations and travel distances. Together these results suggest that both  
488 the hypsometry and the width function of a wide range of catchments can be approximated to first order  
489 using the framework developed here, provided that variations in the channel profile can be modeled.

## 490 5.2 Future research opportunities

491 Our results suggest many potentially fruitful avenues for future research. First, joint distributions  
492 of travel distance and elevation, combined with knowledge of rates of precipitation, erosion or other  
493 material fluxes, can be used to understand how energy is created and dissipated across landscapes. The  
494 concept of source-area power provides a quantitative measure of the spatial distribution of processes that  
495 influence the supply of materials to the catchment outlet. For example, this framework can be used to  
496 understand how the size distribution of sediments passing through the catchment outlet is influenced by  
497 weathering conditions at source elevations (Riebe et al., 2015), and by particle breakdown in transport  
498 (Attal and Lave, 2009). Catchment power, the integral of source-area power over the whole catchment,  
499 provides a metric for comparisons between catchments, and could be used to quantify, and help explain, the  
500 variation in topography across gradients in climate, tectonics and lithology.

501 A second set of research questions emerges from our approach to modeling synthetic joint  
502 distributions of elevation and transport distance. What explains the common tendency for positive skew in  
503 the distribution of area with elevation for a given travel distance? What do differences in the strength of  
504 this asymmetry from one catchment to another tell us about landscape-forming processes? Why are area  
505 and local relief within a travel distance bin linearly proportional, and does this relationship hold across a



506 wider suite of catchments? Can the model of a fully synthetic catchment be used to represent landscapes  
507 across greater ranges of relief and drainage area than explored here?

508 Finally, the apparent success of our empirical model in capturing the bulk trends in the joint  
509 distribution of elevation and travel distance in our study catchments suggests that there may be value in  
510 developing a more comprehensive model, which accounts explicitly for the branching structure of the  
511 channel network. Such a model might have at its core a representation of the distribution of elevation and  
512 travel distance for a first-order catchment similar to our empirical model for Inyo Creek. The model would  
513 then represent larger catchments as combinations of multiple first-order headwater sub-catchments, and the  
514 hillslope facets that drain directly to higher-order channel segments. This raises the question of whether  
515 there is a characteristic distribution of elevation for a given travel distance in the facets draining higher-  
516 order valley slopes, and does it differ from the headwater sub-catchments in the same landscape? Variation  
517 in the topology of branching networks will shift the relative contributions of headwater sub-catchments and  
518 higher-order facets to the number of source-areas at a given elevation or travel distance. How sensitive are  
519 the distributions of source-area power to variations in network topology? Ultimately, such a model may  
520 help explain both the central tendency and variability in the joint distribution of elevation and travel  
521 distance, and provide a stronger theoretical foundation for understanding both the three-dimensional  
522 structure of catchment topography.

## 523 **6 Summary**

524 Here we showed that the joint distribution of elevation and travel distance provides fresh  
525 perspective on the vertical and horizontal structure of catchments in mountain landscapes (Fig. 4). In  
526 particular, we showed that the paired values of elevation and travel distance can be collapsed into a single  
527 index – the mean slope along the travel path – which varies both within and across catchments (Fig. 5).  
528 Mean slope can be combined with knowledge of the fluxes and density of materials produced at, or  
529 delivered to source areas, to define source-area power, and its integral catchment power, new metrics for  
530 quantifying spatial variations in hydrologic and geomorphic processes within and between catchments (Fig.  
531 6). To enable modeling of processes influenced by source-area power, we developed an empirical statistical  
532 framework for defining the joint distribution of elevation and travel distance. We used the Inyo Creek  
533 catchment as a prototype, and found that the distribution of elevation between the main-stem channel and  
534 ridge profiles, for a given travel distance bin, is well-represented by a parameterization of the beta  
535 distribution. To define a fully synthetic catchment, we derived power-law and exponential expressions for  
536 the channel and ridge profiles, which when combined with the model for elevation distribution, can  
537 produce realistic hypsometric curves and width functions. Key questions emerging from this work include:  
538 how do patterns of source-area and catchment power vary across spatial gradients in climate, tectonics and  
539 lithology? What explains the characteristic skew of elevation distributions for a given travel distance? And



540 how do the distributions of source-area and catchment power arise from the branching properties of  
541 networks and the relief structure of landscapes.

## 542 **Appendix A: Derivation of channel and ridge profile equations**

### 543 **A.1 Main-stem channel power-law profile**

544 To create an expression for the longitudinal profile of the main-stem channel, we coupled the  
545 widely observed power-law scaling between slope ( $S$ ) and drainage area ( $A$ )

$$546 \quad S = k_s A^{-\theta} \quad (\text{A1})$$

547 and the likewise common power-law scaling of main-stem distance ( $L$ ) and area

$$548 \quad A = k_A L^H \quad (\text{A2}).$$

549 In Equation A1, known as Flint's law,  $k_s$  and  $\theta$  are empirical coefficients (where  $\theta$  is referred to as profile  
550 concavity). In Equation A2, a version of Hack's law,  $L$  is a local distance downstream from the catchment  
551 divide along the main-stem valley axis, and  $k_A$  and  $H$  are empirical coefficients (with  $H$  the reciprocal of the  
552 Hack exponent). Hack's law can also be written in terms of the local travel distance upstream of the  
553 catchment outlet,  $x$ ,

$$554 \quad A = k_A (L_{\max} - x)^H \quad (\text{A3})$$

555 where  $L_{\max}$  is the value of  $L$  at the outlet (i.e.,  $x = L_{\max} - L$ ).

556 Combining equations A1 and A3 we obtain an expression for mainstem channel slope,  $S_c$ , as a  
557 function of distance upstream  $x$

$$558 \quad S_c = \frac{\partial z_c}{\partial x} = k_s k_A^{-\theta} (L_{\max} - x)^{-\theta H} \quad (\text{A4})$$

559 where  $z_c$  is the elevation of the mainstem channel.

560 Integrating equation A4 provides an expression for the mainstem longitudinal profile

$$561 \quad z_c = k_c \left[ (L_{\max})^{1-\theta H} - (L_{\max} - x)^{1-\theta H} \right] \quad (\text{A5a})$$

562 where

$$563 \quad k_c = \frac{k_s k_A^{-\theta}}{1 - \theta H} \quad (\text{A5b})$$



564 Equation A5 is valid for the fluvial portion of the channel network. However, at small drainage  
 565 areas, and the fluvial slope-area scaling (Eqn. A1) does not apply. Typically, slope changes much less  
 566 rapidly as drainage changes in this part of the landscape. For simplicity we assume that slope is constant  
 567 above a point on the longitudinal profile that we refer to as the channel head.

568 We define a distance  $L_{ch}$  which is the travel distance from where the valley axis meets the drainage  
 569 divide down to the channel head; subscript  $ch$  indicates channel head. The elevation at the channel head,  
 570 where  $x = x_{ch} = (L_{max} - L_{ch})$  is

$$571 \quad z_C = k_C \left[ (L_{max})^{1-\theta H} - (L_{ch})^{1-\theta H} \right] \quad (A6).$$

572 The drainage area at the channel head  $A_{ch}$  is

$$573 \quad A_{ch} = k_A L_{ch}^H \quad (A7)$$

574 and the constant gradient above this point  $S_h$  is

$$575 \quad S_h = k_s A_{ch}^{-\theta} = \frac{k_s}{k_A^\theta} L_{ch}^{-\theta H} \quad (A8)$$

576 Thus the elevation of the long profile, from bottom to top can be written as follows:

$$577 \quad z_C = k_C \left[ (L_{max})^{1-\theta H} - (L_{max} - x)^{1-\theta H} \right] \text{ for } 0 \leq x \leq x_{ch} \quad (A9)$$

$$578 \quad z_C = k_C \left[ (L_{max})^{1-\theta H} - (L_{ch})^{1-\theta H} \right] + S_h (x - x_{ch}) \quad \text{for } x_{ch} < x \leq L_{max} \quad (A10)$$

579 The highest point along the mainstem profile,  $z_{C\_max}$  is

$$580 \quad z_{C\_max} = k_C \left[ (L_{max})^{1-\theta H} - (L_{ch})^{1-\theta H} \right] + S_h L_{ch} \quad (A11)$$

## 581 A.2 Ridge power-law profile

582 To define the ridge long profile, we assume a simple power-law relation between elevation and  
 583 distance,

$$584 \quad z_R = k_R x^P \quad (A12)$$

585 where  $k_R$  is an adjustable parameter and the exponent  $P$  depends on the parameters of the channel profile.

586 To specify  $P$  we impose the constraints that the ridge profile must intersect the mainstem channel profile at  
 587 the two end points, where  $x = 0$  and  $x = L_{max}$ , the lowest and highest points in the landscape.





588 With the constraints that the elevation of the ridge  $z_r$  and the channel  $z_c$  match where  $x = 0$  and  $x =$   
 589  $L_{max}$ , we can solve for the exponent  $P$  as follows:

$$590 \quad P = \frac{\log(z_{c\_max}/k_R)}{\log(L_{max})} \quad (A13)$$

591 Thus, the ridge network and the channel network are pinned together at the two end points.

### 592 A.3 Inyo Creek power-law profile parameters

593 The combined model for the ridge and channel profiles has 6 parameters; all other values are  
 594 calculated from the equations above. For the Inyo Creek channel and ridge profiles extracted from the  
 595 distributions of elevation for travel distances binned in 50 meter increments, Table A1 lists one possible set  
 596 of values that adequately reproduce the observed profile. These values were tuned to satisfy the following  
 597 constraints:  $L_{max} = 4700$  m, the range of travel distances of Inyo rounded to nearest 50 m; drainage area at  
 598 outlet =  $3.4 \text{ km}^2$ ; maximum elevation above outlet of 1890 m

### 599 A.4 Main-stem channel exponential profile

600 Exponential profiles have been used by many, including Hack (cites). Simply state elevation of the  
 601 channel as increasing exponentially with distance upstream of the outlet

$$602 \quad z_c = k_e e^{\lambda x} \quad (A14)$$

603 where  $k_e$  and lambda are empirical coefficients. As with the power profile, this is only valid between the  
 604 outlet and the channel head, where for simplicity we assume the slope becomes uniform. For the  
 605 exponential profile (equation A14), the channel slope

$$606 \quad S_c = \frac{\partial z}{\partial x} = \lambda k_e e^{\lambda x} \quad (A15)$$

607 grows too slowly with increasing distance upstream of the channel head to represent the steep headwater  
 608 valley axis slope, so we define  $S_{h\_exp}$  as an independent empirical model constant, with the constraint is  
 609 that it must be greater than the slope of the exponential profile at the channel head

$$610 \quad S_{h\_exp} > S_{c\_max} = \lambda k_e e^{\lambda(L_{max}-L_{ch})} \quad (A16).$$

611 The full channel profile expression becomes

$$612 \quad z_c = k_e e^{\lambda x} \quad \text{for } 0 \leq x \leq x_{ch} \quad (A17a)$$



$$613 \quad z_c = k_e e^{\lambda x_{ch}} + S_{h\_exp} (x - x_{ch}) \quad \text{for } x_{ch} < x \leq L_{max} \quad (A17b)$$

614 and the highest point along the mainstem profile,  $Z_{C\_max}$  is

$$615 \quad z_{c\_max} = k_e e^{\lambda x_{ch}} + S_{h\_exp} L_{ch} \quad (A18).$$

### 616 A.5 Ridge exponential profile

617 To define the ridge long profile, for symmetry with the channel profile we assume an exponential  
 618 relation between elevation and distance,

$$619 \quad z_R = k_{Re} e^{\gamma x} \quad (A19)$$

620 Where the coefficient  $k_{Re}$  is an adjustable parameter, and the exponent  $\gamma$  depends on the parameters of the  
 621 channel profile. As with the power law profile derivation, to specify  $\gamma$  we impose the constraints that the  
 622 ridge profile must intersect the mainstem channel profile at the two end points, where  $x = 0$  and  $x = L_{max}$ ,  
 623 the lowest and highest points in the landscape.

624 With the constraints that the elevation of the ridge  $z_r$  and the channel  $z_c$  match where  $x = L_{max}$ , we  
 625 can solve for the exponent  $\gamma$

$$626 \quad \gamma = \frac{\ln(z_{c\_max} / k_{Re})}{L_{max}} \quad (A20)$$

627 The ridge network and the channel network are pinned together at these two end points.

### 628 A.6 Inyo Creek exponential profile parameters

629 The combined model for the two exponential profiles has five parameters; all other values are  
 630 calculated from the equations above. Table A2 lists one possible best fit (by eye) set of values for the Noyo  
 631 River channel and ridge profiles extracted from the distributions of elevation for travel distances binned in  
 632 250 meter increments. These values were tuned to satisfy the following constraints:  $L_{max} = 20,750$  m, the  
 633 range of travel distances of Inyo rounded to nearest 50 m; maximum elevation above outlet = 620 m (along  
 634 mainstem profile).

### 635 Data Availability

636 The DEMs used in this paper can be obtained upon request from the corresponding author.

637



638 **Acknowledgments**

639 We thank Sarah Konrad and Catherine Noll for contributing to preliminary DEM analysis. Funding was  
640 provided by the Doris and David Dawdy Fund for Hydrologic Research, and National Science Foundation  
641 Grants EAR 1325033 and 1239521.

642 **References**

- 643 Algeo, T. J., & Sclafnin, K. B. (1995). Reconstructing eustatic and epeirogenic trends from Paleozoic  
644 continental flooding records. In *Sequence Stratigraphy and Depositional Response to Eustatic,  
645 Tectonic and Climatic Forcing* (pp. 209-246). Springer Netherlands.
- 646 Attal, M., & Lavé, J. (2006). Changes of bedload characteristics along the Marsyandi River (central Nepal):  
647 Implications for understanding hillslope sediment supply, sediment load evolution along fluvial  
648 networks, and denudation in active orogenic belts. *Geological Society of America Special  
649 Papers*, 398, 143-171.
- 650 Bales, R.C., Hopmans, J.W., O'Geen, A.T., Meadows, M., Hartsough, P.C., Kirchner, P., Hunsaker, C.T.  
651 and Beaudette, D., 2011. Soil moisture response to snowmelt and rainfall in a Sierra Nevada  
652 mixed-conifer forest. *Vadose Zone Journal*, 10(3), pp.786-799.
- 653 Brocklehurst, S. H., & Whipple, K. X. (2002). Glacial erosion and relief production in the Eastern Sierra  
654 Nevada, California. *Geomorphology*, 42(1), 1-24.
- 655 Brocklehurst, S. H., & Whipple, K. X. (2004). Hypsometry of glaciated landscapes. *Earth Surface  
656 Processes and Landforms*, 29(7), 907-926.
- 657 Brozović, N., Burbank, D. W., & Meigs, A. J. (1997). Climatic limits on landscape development in the  
658 northwestern Himalaya. *Science*, 276(5312), 571-574.
- 659 Burbank, D. W., Blythe, A. E., Putkonen, J., Pratt-Sitaula, B. G. A. B. E. T., Gabet, E., Oskin, M., ... &  
660 Ojha, T. P. (2003). Decoupling of erosion and precipitation in the Himalayas. *Nature*, 426(6967),  
661 652-655.
- 662 Burns, J. W. (1972). Some effects of logging and associated road construction on northern California  
663 streams. *Transactions of the American Fisheries Society*, 101(1), 1-17.
- 664 Coulthard, T. J. (2001). Landscape evolution models: a software review. *Hydrological processes*, 15(1),  
665 165-173.
- 666 Dai, J. J., Lorenzato, S., & Rocke, D. M. (2004). A knowledge-based model of watershed assessment for  
667 sediment. *Environmental Modelling & Software*, 19(4), 423-433.
- 668 Gaillardet, J., Dupré, B., & Allègre, C. J. (1999). Geochemistry of large river suspended sediments: silicate  
669 weathering or recycling tracer?. *Geochimica et Cosmochimica Acta*, 63(23), 4037-4051.
- 670 Goulden, M. L., & Bales, R. C. (2014). Mountain runoff vulnerability to increased evapotranspiration with  
671 vegetation expansion. *Proceedings of the National Academy of Sciences*, 111(39), 14071-14075.



- 672 Gupta, V. K., & Mesa, O. J. (1988). Runoff generation and hydrologic response via channel network  
673 geomorphology—Recent progress and open problems. *Journal of hydrology*, 102(1), 3-28.
- 674 Gupta, V. K., & Waymire, E. D. (1989). Statistical self-similarity in river networks parameterized by  
675 elevation. *Water Resources Research*, 25(3), 463-476.
- 676 Hahm, W. J., Riebe, C. S., Lukens, C. E., & Araki, S. (2014). Bedrock composition regulates mountain  
677 ecosystems and landscape evolution. *Proceedings of the National Academy of Sciences*, 111(9),  
678 3338-3343.
- 679 Holbrook, W. S., Riebe, C. S., Elwaseif, M., L Hayes, J., Basler-Reeder, K., L Harry, D., ... & W  
680 Hopmans, J. (2014). Geophysical constraints on deep weathering and water storage potential in  
681 the Southern Sierra Critical Zone Observatory. *Earth Surface Processes and Landforms*, 39(3),  
682 366-380.
- 683 Hunsaker, C. T., & Neary, D. G. (2012). Sediment loads and erosion in forest headwater streams of the  
684 Sierra Nevada, California. In *Proceedings of a workshop for the International Association of*  
685 *Hydrological Sciences, General Assembly in Melbourne. Revisiting Experimental Catchment*  
686 *Studies in Forest Hydrology*. Wallingford, United Kingdom (pp. 195-204).
- 687 Hunsaker, C. T., Whitaker, T. W., & Bales, R. C. (2012). Snowmelt runoff and water yield along elevation  
688 and temperature gradients in California's Southern Sierra Nevada1.
- 689 Jin, L., Ravella, R., Ketchum, B., Bierman, P. R., Heaney, P., White, T., & Brantley, S. L. (2010). Mineral  
690 weathering and elemental transport during hillslope evolution at the Susquehanna/Shale Hills  
691 Critical Zone Observatory. *Geochimica et Cosmochimica Acta*, 74(13), 3669-3691.
- 692 Lashermes, B., & Foufoula-Georgiou, E. (2007). Area and width functions of river networks: New results  
693 on multifractal properties. *Water resources research*, 43(9).
- 694 Leithold, E. L., Blair, N. E., & Perkey, D. W. (2006). Geomorphologic controls on the age of particulate  
695 organic carbon from small mountainous and upland rivers. *Global Biogeochemical Cycles*, 20(3).
- 696 Lifton, N. A., & Chase, C. G. (1992). Tectonic, climatic and lithologic influences on landscape fractal  
697 dimension and hypsometry: implications for landscape evolution in the San Gabriel Mountains,  
698 California. *Geomorphology*, 5(1), 77-114.
- 699 Lisle, T. E. (1982). Effects of aggradation and degradation on riffle-pool morphology in natural gravel  
700 channels, northwestern California. *Water Resources Research*, 18(6), 1643-1651.
- 701 Lomolino, M. A. R. K. (2001). Elevation gradients of species-density: historical and prospective  
702 views. *Global Ecology and Biogeography*, 10(1), 3-13.
- 703 Marshall, J. A., & Sklar, L. S. (2012). Mining soil databases for landscape-scale patterns in the abundance  
704 and size distribution of hillslope rock fragments. *Earth Surface Processes and Landforms*, 37(3),  
705 287-300.
- 706 Minder, J. R., Durran, D. R., & Roe, G. H. (2011). Mesoscale controls on the mountainside snow  
707 line. *Journal of the Atmospheric Sciences*, 68(9), 2107-2127.



- 708 Moussa, R. (2008). What controls the width function shape, and can it be used for channel network  
709 comparison and regionalization?. *Water Resources Research*, 44(8).
- 710 Nash, J., & Sutcliffe, J. V. (1970). River flow forecasting through conceptual models part I—A discussion  
711 of principles. *Journal of hydrology*, 10(3), 282-290.
- 712 PRISM Climate Group, (2014) Oregon State University, <http://prism.oregonstate.edu>.
- 713 Raich, J. W., Russell, A. E., & Vitousek, P. M. (1997). Primary productivity and ecosystem development  
714 along an elevational gradient on Mauna Loa, Hawai'i. *Ecology*, 78(3), 707-721.
- 715 Reiners, P. W., Ehlers, T. A., Mitchell, S. G., & Montgomery, D. R. (2003). Coupled spatial variations in  
716 precipitation and long-term erosion rates across the Washington Cascades. *Nature*, 426(6967),  
717 645-647.
- 718 Richey, J. E., Mertes, L. A., Dunne, T., Victoria, R. L., Forsberg, B. R., Tancredi, A. C., & Oliveira, E.  
719 (1989). Sources and routing of the Amazon River flood wave. *Global biogeochemical cycles*, 3(3),  
720 191-204.
- 721 Riebe, C. S., Kirchner, J. W., & Finkel, R. C. (2004). Erosional and climatic effects on long-term chemical  
722 weathering rates in granitic landscapes spanning diverse climate regimes. *Earth and Planetary  
723 Science Letters*, 224(3), 547-562.
- 724 Reibe, C.S., L.S. Sklar, C.E. Lukens, and D.L. Shuster (2015). Climate and topography control the size of  
725 sediment produced on mountain slopes, *Proceedings of the National Academy of Sciences*, doi:  
726 10.1073/pnas.1503567112.
- 727 Rigon, R., Rinaldo, A., & Rodriguez - Iturbe, I. (1994). On landscape self - organization. *Journal of  
728 Geophysical Research: Solid Earth* (1978–2012), 99(B6), 11971-11993.
- 729 Rigon, R., Bancheri, M., Formetta, G., & de Lavenne, A. (2015). The geomorphological unit hydrograph  
730 from a historical - critical perspective. *Earth Surface Processes and Landforms*.
- 731 Rinaldo, A., Vogel, G. K., Rigon, R., & Rodriguez - Iturbe, I. (1995). Can one gauge the shape of a  
732 basin?. *Water Resources Research*, 31(4), 1119-1127.
- 733 Roe, G. H. (2005). Orographic precipitation. *Annu. Rev. Earth Planet. Sci.*, 33, 645-671.
- 734 Sklar, L. S., Dietrich, W. E., Fofoula - Georgiou, E., Lashermes, B., & Bellugi, D. (2006). Do gravel bed  
735 river size distributions record channel network structure?. *Water Resources Research*, 42(6).
- 736 Stock, G. M., Ehlers, T. A., & Farley, K. A. (2006). Where does sediment come from? Quantifying  
737 catchment erosion with detrital apatite (U-Th)/He thermochronometry. *Geology*, 34(9), 725-728.
- 738 Strahler, A. N. (1952). Hypsometric (area-altitude) analysis of erosional topography. *Geological Society of  
739 America Bulletin*, 63(11), 1117-1142.
- 740 Taylor, B. R., & Chauvet, E. E. (2014). Relative influence of shredders and fungi on leaf litter  
741 decomposition along a river altitudinal gradient. *Hydrobiologia*, 721(1), 239-250.
- 742 Tarboton, D. G. (1997). A new method for the determination of flow directions and upslope areas in grid  
743 digital elevation models. *Water resources research*, 33(2), 309-319.



- 744 Tucker, G. E., & Hancock, G. R. (2010). Modelling landscape evolution. *Earth Surface Processes and*  
745 *Landforms*, 35(1), 28-50.
- 746 Wahrhaftig, C. (1965). Stepped topography of the southern Sierra Nevada, California. *Geological Society*  
747 *of America Bulletin*, 76(10), 1165-1190.
- 748 White, A. F., & Blum, A. E. (1995). Effects of climate on chemical\_ weathering in watersheds. *Geochimica*  
749 *et Cosmochimica Acta*, 59(9), 1729-1747.
- 750 Willgoose, G. (2005). Mathematical modeling of whole landscape evolution. *Annu. Rev. Earth Planet.*  
751 *Sci.*, 33, 443-459.

## 752 **Figure captions**

753 **Figure 1. Study site locations and comparison of channel and ridge profiles.** Left: Location map of  
754 study catchments in California, USA. Right: Profiles of the lowest point at each travel distance (i.e., the  
755 mainstem channel) and the highest point at each travel distance (referred to here as the ridge profile). The  
756 channel and ridge profiles enclose all paired values of elevation and travel distance for each catchment.  
757 Differences in catchment relief and size across the sites produce distinct populations of paired values. The  
758 ratio of elevation to travel distance is the mean slope along a path from the source to the catchment outlet.  
759 Thus the catchments also harbor distinct populations of mean slope.

760 **Figure 2. Spatial distributions of elevation and travel distance.** Maps showing the spatial distribution of  
761 elevation and travel distributions across the Inyo Creek (A), Providence Creek (B), and Noyo River (C)  
762 study catchments. Black lines are elevation contours, with hillshade in background for emphasis. Color  
763 shade shows scaled values of travel distance (normalized by the maximum value in the catchment). Note  
764 variation in scale and compass orientation from one watershed to the next. Elevation contour spacing is 50  
765 m in (C) and (B), and 200 m in (C).

766 **Figure 3. Hypsometry and width functions.** Normalized frequency distributions of elevation (a) and  
767 travel distance to the outlet (b). Frequencies are normalized so that the area under the curve is equal to 1 in  
768 each case. Binning increment is 1/47 of maximum value (Table 1).

769 **Figure 4. Joint distributions of elevation and travel distance.** Distribution of source area elevations and  
770 travel distances from 10 m DEMs of catchments drained by (a) Inyo Creek, (b) Providence Creek, and (c)  
771 the Noyo River. Bivariate frequency distributions of elevation and travel distance for each catchment (d-f)  
772 show relative density (color bar in (d)); data binning as in Figure 2.

773 **Figure 5. Distribution of mean slope across catchments.** Histograms (insets, A-C) of mean slope along  
774 travel path from source to outlet (ratio of source area elevation to travel distance), with colors highlighting  
775 bins of relatively low, medium and high values. Bins of common mean slope form linear bands on plots of  
776 elevation versus travel distance (A-C). Maps of catchments (D-F) show spatial distribution of source areas  
777 sharing similar mean slope for highlighted values.



778 **Figure 6. Spatial distribution of source-area power for water and sediment.** Histograms (left) of  
779 source-area power calculated using equation 3 for the Inyo Creek catchment for water delivered by  
780 precipitation (A), and sediment produced by erosion (B). Panel (C) shows dimensionless ratio of source-  
781 area water power to sediment production rate (eqn. 4); colors highlight bins of relatively low, medium and  
782 high values. Maps (right) show spatial distribution of highlighted values. Note the sharp increase in water  
783 power per sediment flux from upper to lower parts of the catchment.

784 **Figure 7. Elevation distributions for different travel distances at Inyo Creek.** (A) Elevation data points  
785 for Inyo Creek catchment parsed into forty-seven 100-m wide travel distance bins. (B) Distributions of  
786 elevation for seven representative travel distance bins; colors correspond to shaded bins in panel A, mean  
787 travel distance indicated for each curve. (C) Fraction of total area in each travel distance bin as a function  
788 of fraction of total relief in each bin, roughly follows 1:1 line, colored symbols indicate representative bins  
789 in panels A and B. (D) Collapse of elevation distributions for each travel distance bin, with elevation  
790 normalized by relief within bin and area by total area within bin. Best-fit beta distribution captures typical  
791 shape of hypsometry for a given travel distance.

792 **Figure 8. Objective function for best-fit beta distribution shape parameters.** Contour plot of root mean  
793 sum of squared error (RMSE) between actual and predicted area density of elevation for a given travel  
794 distance for paired values of beta distribution shape parameters. Minimum RMSE at  $\alpha = 2.6$  and  
795  $\beta = 3.4$  as indicated by diamond. In this example, travel distance and elevation bin sizes equal 100 m and  
796 40 m respectively.

797 **Figure 9. Model performance.** Variation in Nash-Sutcliffe model efficiency statistic (Eqn. 8) with size of  
798 travel distance and elevation bins, for modeled joint distributions of elevation and travel distance for Inyo  
799 Creek, using actual profiles (solid lines) and modeled profiles (dashed lines). Nash-Sutcliffe value of 1.0  
800 indicates perfect agreement between modeled and actual distribution of area; value of 0 indicates model  
801 performance no better than uniform distribution of mean area density. A trade-off between model  
802 efficiency and spatial resolution is revealed by trend toward higher Nash-Sutcliffe values for larger bin sizes.

803 **Figure 10. Normalized Distribution of elevation by travel distance bin for other catchments.** Travel  
804 distance and elevation bin sizes = 1/20 of maximum values. Thin lines show elevation distributions,  
805 normalized by local relief, for each travel distance bin. Thick colored curves show best-fit beta  
806 distributions, with shape parameter values indicated. Normalized elevation distributions are more skewed  
807 for Noyo River, reflecting larger drainage area and greater degree of landscape dissection.

808 **Figure 11. Fully synthetic joint distribution of elevation and travel distance for catchment the size of**  
809 **Inyo Creek.** In (A) channel and ridge profiles are defined by equations 9 and 10, area density (color bar)  
810 given by equations 7 and 11. Side panels show area density projected on distance axis to create width  
811 function (B) and projected on elevation axis to create hypsometric curve (C).





812 **Figure 12. Comparison of actual with modeled hypsometric curves and width functions for three**  
813 **study catchments.** In each panel, thick colored curves show data from catchment DEM, while thick and  
814 dashed black lines show model predictions using actual and modeled channel and ridge profiles  
815 respectively. Also shown in left panels are hypsometric curves predicted using uniform area distribution,  
816 for the case when Nash-Sutcliffe model efficiency statistic = 0; for this case, predicted width function  
817 matches actual.  
818



819 **Table 1. Study site characteristics**

820		Inyo Creek	Providence Creek	Noyo River
821	Drainage Area (km <sup>2</sup> )	3.4	8.1	144
822	Relief (m)	1,895	1,117	893
823	Max Travel Distance (m)	4,660	7,940	20,790
824	Mean Slope to outlet	0.33	0.14	0.021
825	Elevation of outlet (masl)	2053	998	84
826	Outlet UTM North	392369.717	300456.028	364182.531
827	Outlet UTM East	4049943.32	4101509.08	450994.25

828

829 **Table A1. Inyo Creek power-law profile model parameters**

830	Parameter	Value
831	$\theta$	0.31
832	$H$	1.75
833	$k_s$	25
834	$k_A$	1.28
835	$L_{ch}$	600 m
836	$K_R$	0.6

837

838 **Table A2. Noyo River exponential profile model parameters**

839	Parameter	Value
840	$\lambda$	$1.8 \times 10^{-4} \text{ m}^{-1}$
841	$S_{h\_exp}$	0.16
842	$k_e$	6.7 m
843	$L_{ch}$	2000 m
844	$K_{Re}$	195 m

845

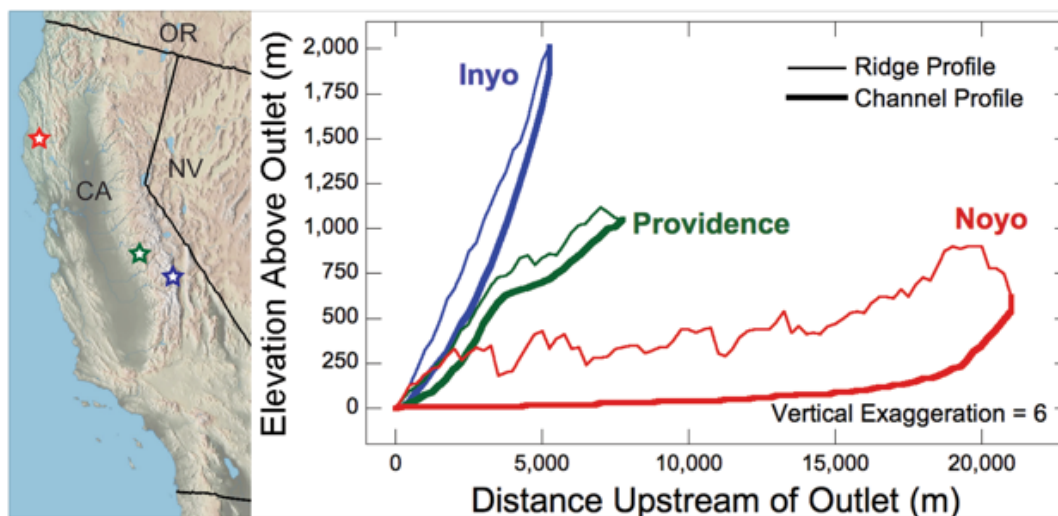


**Figure 1. Study site locations and comparison of channel and ridge profiles.**

Left: Location map of study catchments in California, USA. Right: Profiles of the lowest point at each travel distance (i.e., the mainstem channel) and the highest point at each travel distance (referred to here as the ridge profile). The channel and ridge profiles enclose all paired values of elevation and travel distance for each catchment. Differences in catchment relief and size across the sites produce distinct populations of paired values. The ratio of elevation to travel distance is the mean slope along a path from the source to the catchment outlet. Thus the catchments also harbor distinct populations of mean slope.

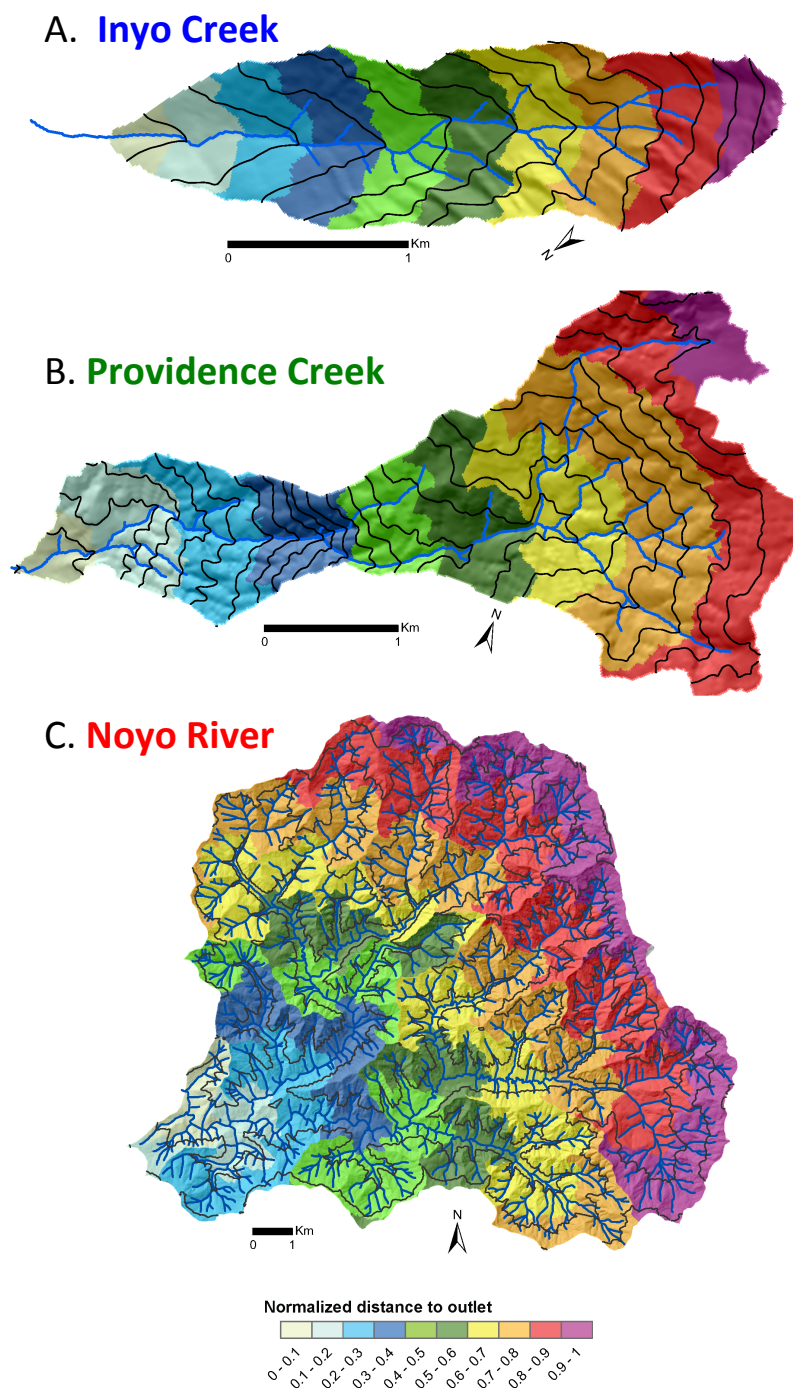


**Figure 2. Spatial distributions of elevation and travel distance.** Maps showing the spatial distribution of elevation and travel distributions across the Inyo Creek (A), Providence Creek (B), and Noyo River (C) study catchments. Black lines are elevation contours, with hillshade in background for emphasis. Color shade shows scaled values of travel distance (normalized by the maximum value in the catchment). Note variation in scale and compass orientation from one watershed to the next. Elevation contour spacing is 50 m in (C) and (B), and 200 m in (A).

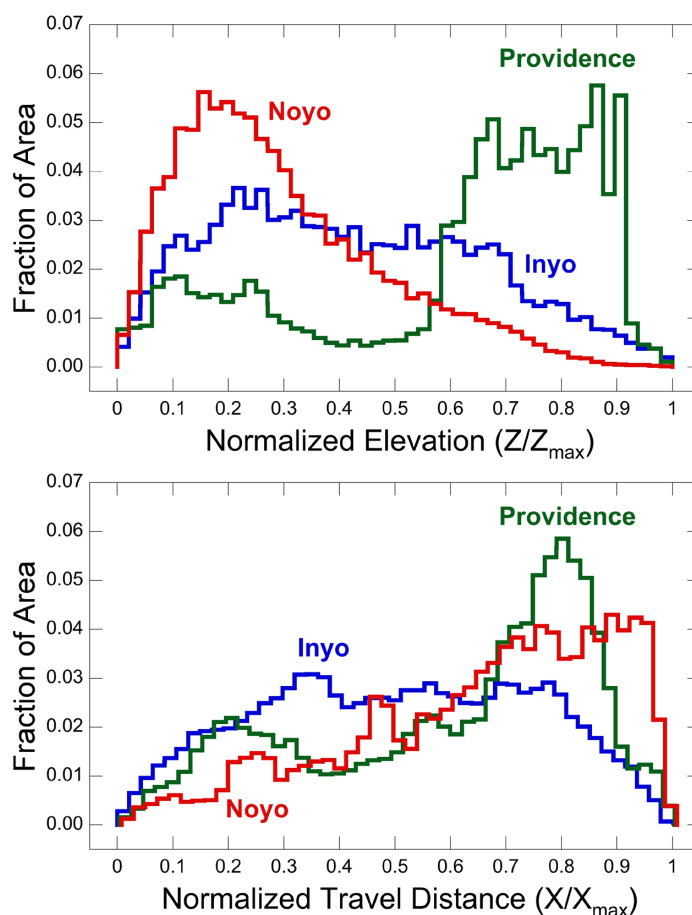


**Figure 3. Hypsometry and width functions.** Normalized frequency distributions of elevation (a) and travel distance to the outlet (b). Frequencies are normalized so that the area under the curve is equal to 1 in each case. Binning increment is  $1/47$  of maximum value (Table 1).

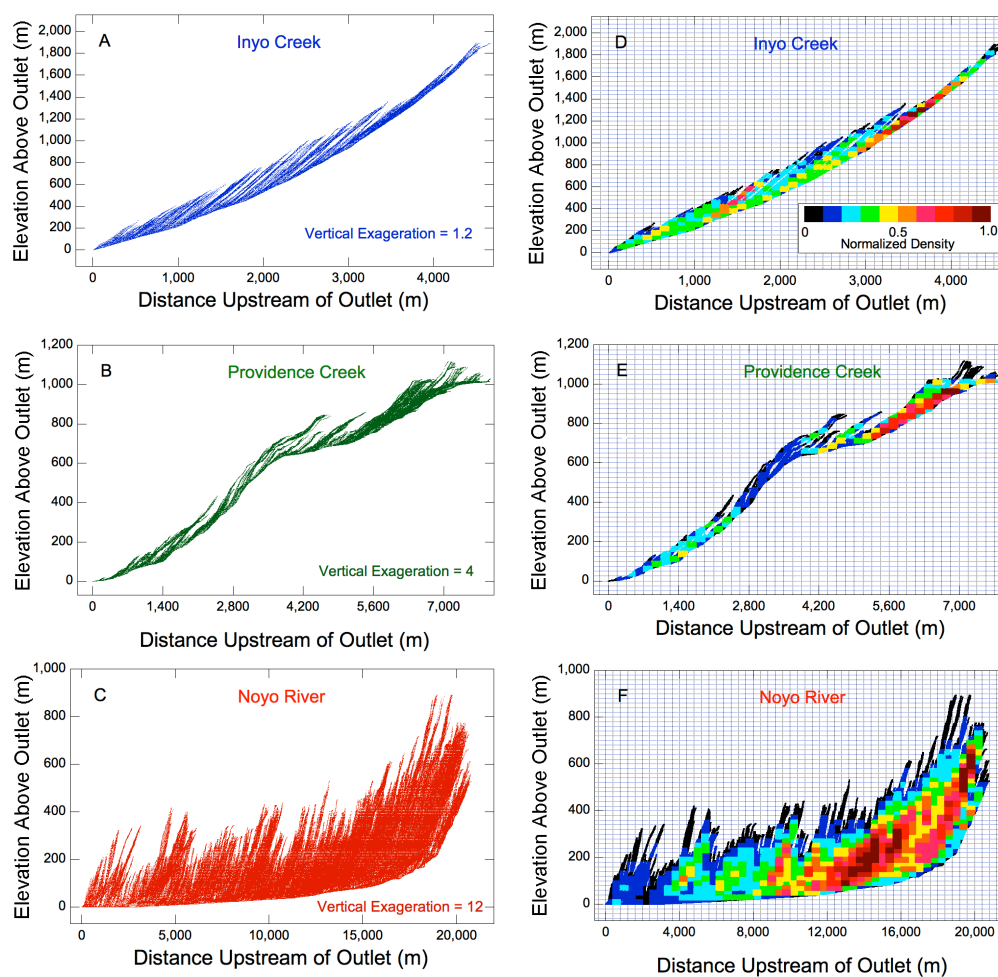


**Figure 4. Joint distributions of elevation and travel distance.**

Distribution of source area elevations and travel distances from 10 m DEMs of catchments drained by (a) Inyo Creek, (b) Providence Creek, and (c) the Noyo River. Bivariate frequency distributions of elevation and travel distance for each catchment (d-f) show relative density (color bar in (d)); data binning as in Figure 2.

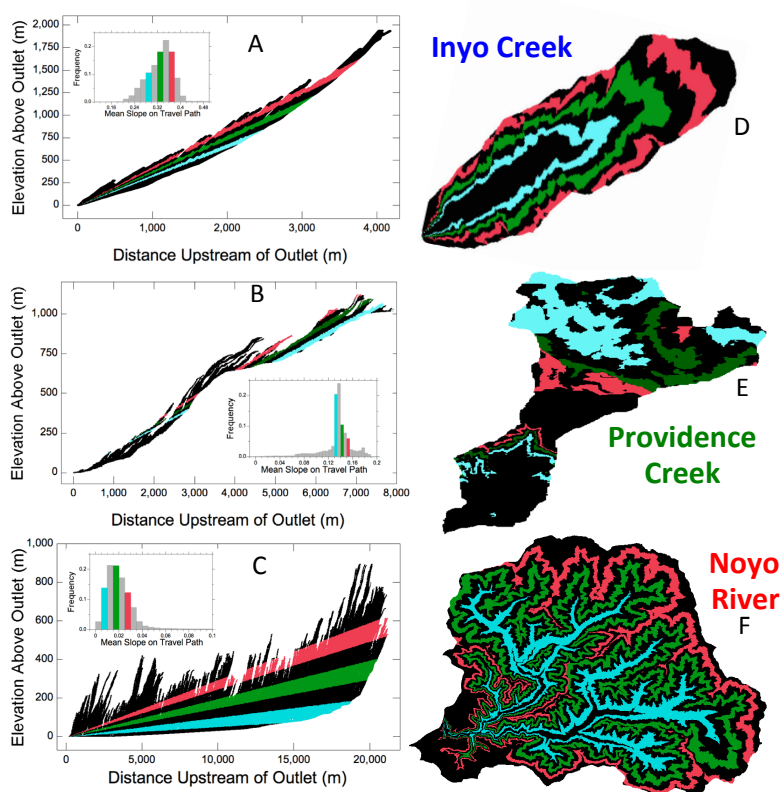


**Figure 5. Distribution of mean slope across catchments.** Histograms (insets, A-C) of mean slope along travel path from source to outlet (ratio of source area elevation to travel distance), with colors highlighting bins of relatively low, medium and high values. Bins of common mean slope form linear bands on plots of elevation versus travel distance (A-C). Maps of catchments (D-F) show spatial distribution of source areas sharing similar mean slope for highlighted values.



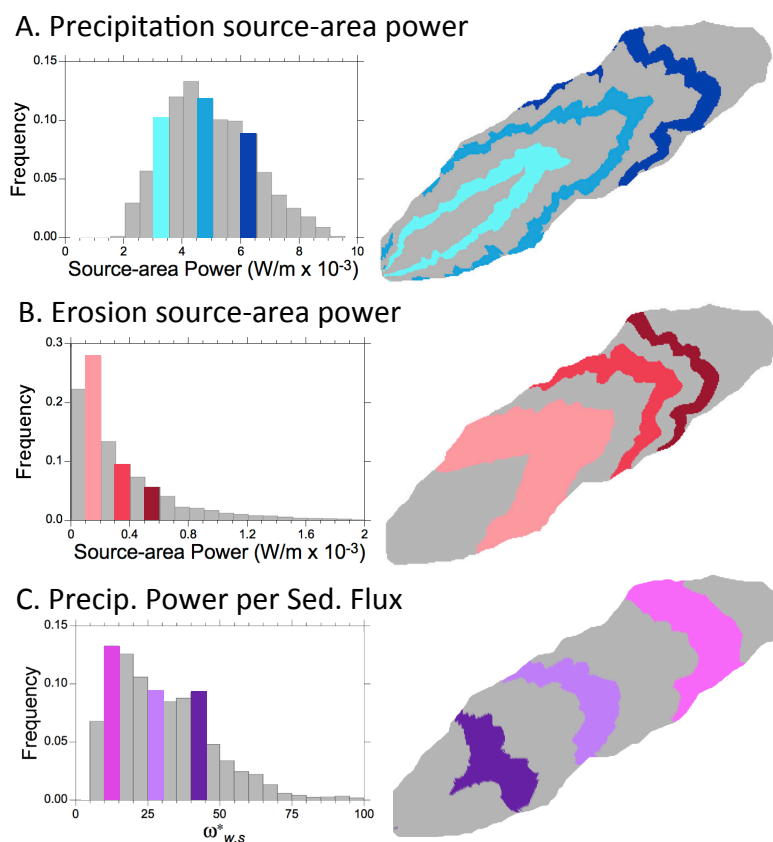


**Figure 6. Spatial distribution of source-area power for water and sediment.** Histograms (left) of source-area power calculated using equation 3 for the Inyo Creek catchment for water delivered by precipitation (A), and sediment produced by erosion (B). Panel (C) shows dimensionless ratio of source-area water power to sediment production rate (eqn. 4); colors highlight bins of relatively low, medium and high values. Maps (right) show spatial distribution of highlighted values. Note the sharp increase in water power per sediment flux from upper to lower parts of the catchment.

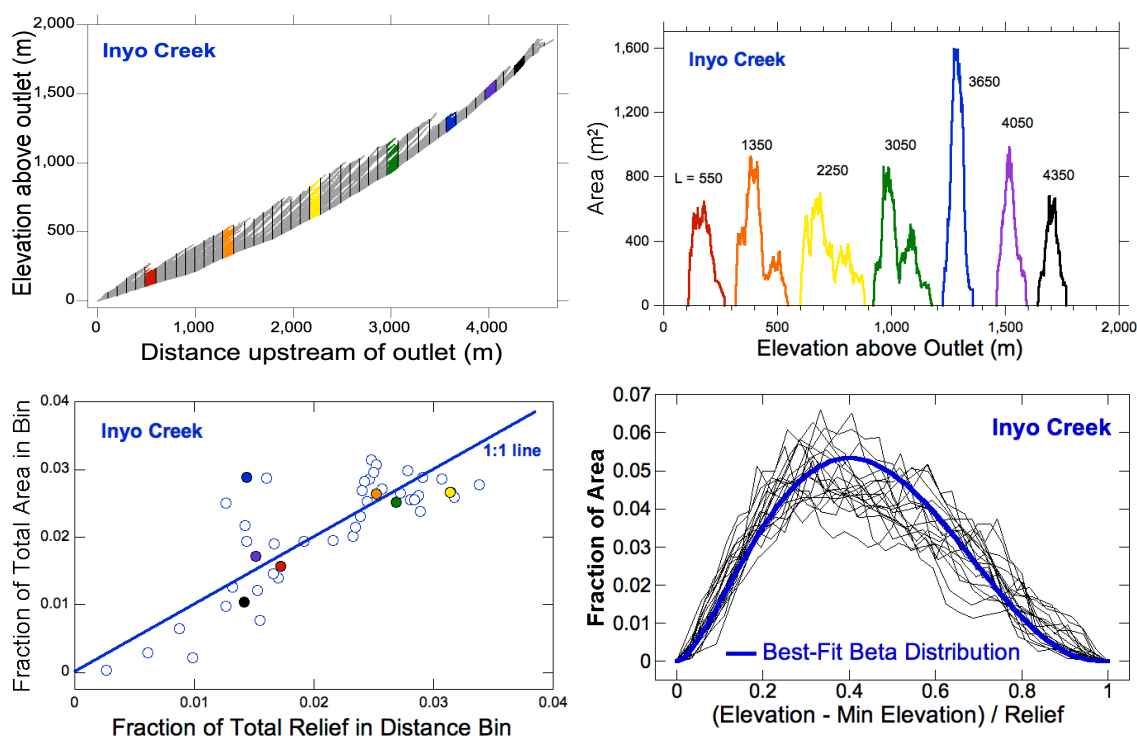


**Figure 7. Elevation distributions for different travel distances at Inyo Creek**

(A) Elevation data points for Inyo Creek catchment parsed into forty seven 100-m wide travel distance bins. (B) Distributions of elevation for seven representative travel distance bins; colors correspond to shaded bins in panel A, mean travel distance indicated for each curve. (C) Fraction of total area in each travel distance bin as a function of fraction of total relief in each bin, roughly follows 1:1 line, colored symbols indicate representative bins in panels A and B. (D) Collapse of elevation distributions for each travel distance bin, with elevation binned in 40 m increments. Elevation is normalized by total relief within distance bin and area normalized by total area within bin. Best-fit beta distribution captures typical shape of hypsometry for a given travel distance.

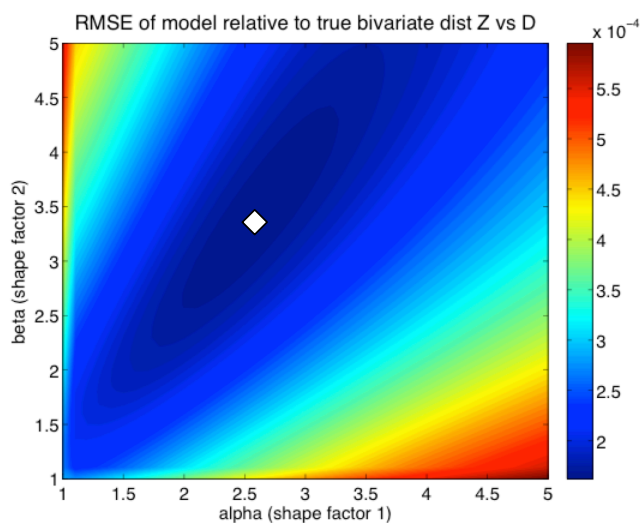


**Figure 8. Objective function for best-fit beta distribution shape parameters**

Contour plot of root mean sum of squared error (RMSE) between actual and predicted area density of elevation for a given travel distance for paired values of beta distribution shape parameters. Minimum RMSE at  $\alpha = 2.6$  and  $\beta = 3.4$  as indicated by diamond. In this example, travel distance and elevation bin sizes equal 100 m and 40 m respectively.

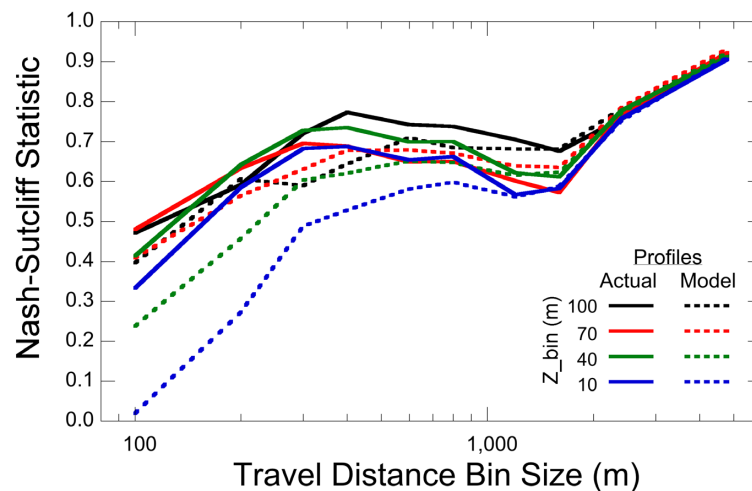


**Figure 9. Model performance.** Variation in Nash-Sutcliffe model efficiency statistic with size of travel distance and elevation bins, for modeled joint distributions of elevation and travel distance for Inyo Creek, using actual profiles (solid lines) and modeled profiles (dashed lines). Nash-Sutcliffe value of 1.0 indicates perfect agreement between modeled and actual distribution of area; value of 0 indicates model performance no better than uniform distribution of mean area density. A trade-off between model efficiency and spatial resolution is revealed by trend toward higher Nash-Sutcliffe values for larger bin sizes.

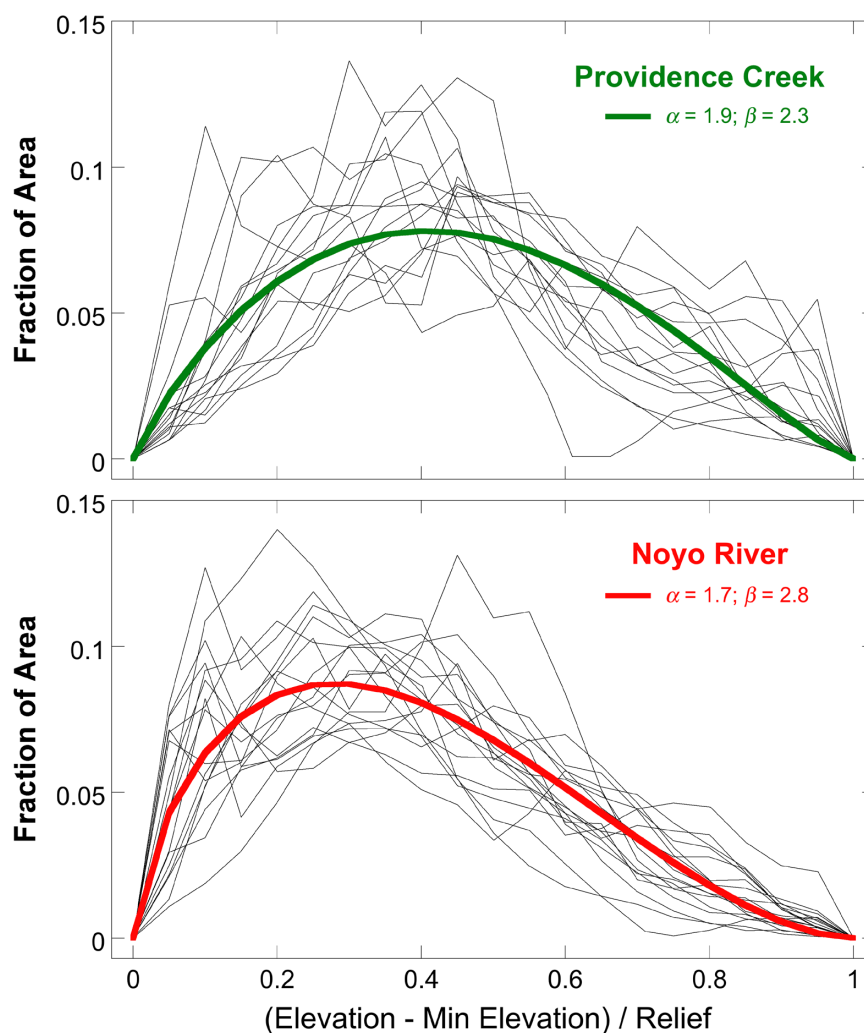


**Figure 10. Normalized Distribution of elevation by travel distance bin for other catchments.** Travel distance and elevation bin sizes = 1/20 of maximum values. Thin lines show elevation distributions, normalized by local relief, for each travel distance bin. Thick colored curves show best-fit beta distributions, with shape parameter values indicated. Normalized elevation distributions are more skewed for Noyo River, reflecting larger drainage area and greater degree of landscape dissection.

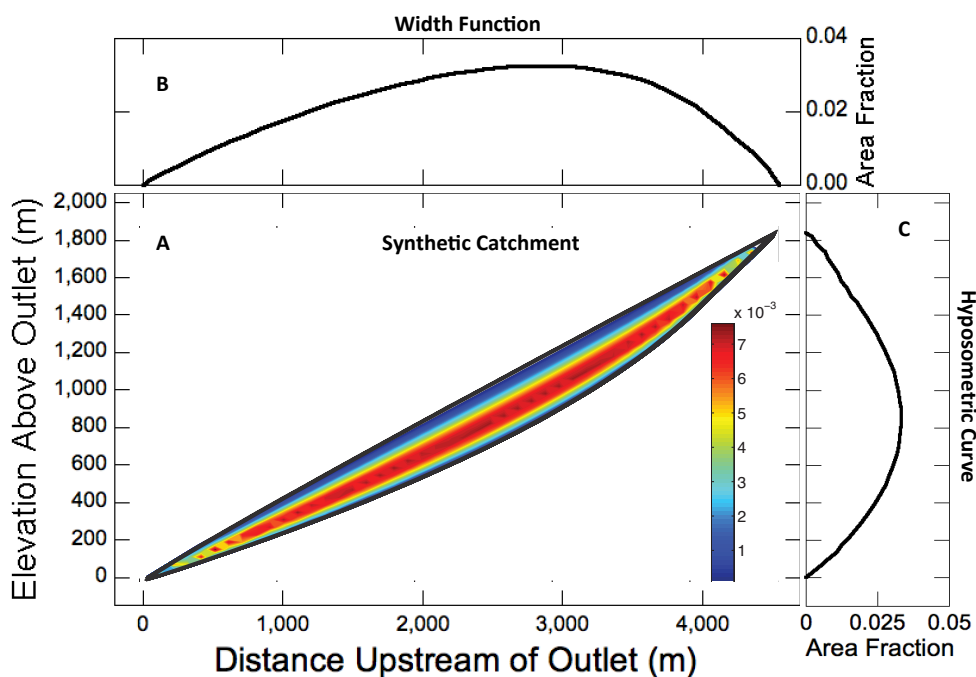


**Figure 11. Fully synthetic joint distribution of elevation and travel distance for catchment the size of Inyo Creek.** In (A) channel and ridge profiles are defined by equations XX and YY, area density (color bar) given by equation ZZ. Side panels show area density projected on distance axis to create width function (B) and projected on elevation axis to create hypsometric curve (C).

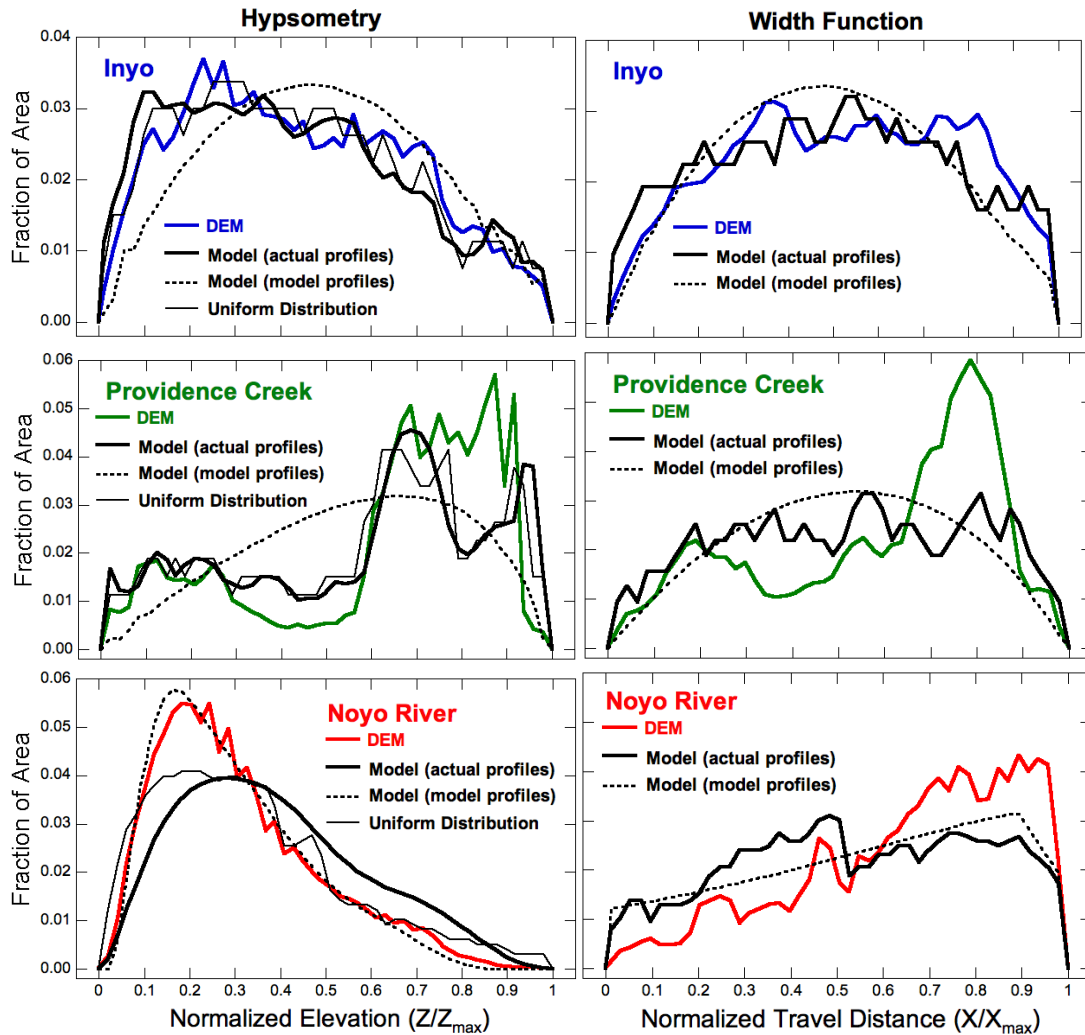


**Figure 12. Comparison of actual with modeled hypsometric curves and width functions for three study catchments.** In each panel, thick colored curves show data from catchment DEM, while thick and dashed black lines show model predictions using actual and modeled channel and ridge profiles respectively. Also shown in left panels are hypsometric curves predicted using uniform area distribution, for the case when Nash-Sutcliffe model efficiency statistic = 0; for this case, predicted width function matches actual.